

Middle Pleistocene environments, landscapes and tephrostratigraphy of the Armenian Highlands: evidence from Bird Farm 1, Hrazdan Valley

JENNI E. SHERRIFF,^{1,2*} KEITH N. WILKINSON,³ POPPY HARDING,¹ HAYLEY HAWKINS,¹ RHYS G. O. TIMMS,¹ DANIEL S. ADLER,⁴ EMILY J. BEVERLY,⁵ SIMON P. E. BLOCKLEY,¹ BORIS GASPARYAN,⁶ CHRISTINA J. MANNING,⁷ DARREN MARK,⁸ SAMVEL NAHAPETYAN⁹ and KATIE J. PREECE¹⁰

¹Centre for Quaternary Research, Department of Geography, Royal Holloway, University of London, UK

²Department of Geography, King's College London, UK

³Department of Archaeology, Anthropology and Geography, University of Winchester, Winchester, UK

⁴Department of Anthropology, University of Connecticut, Storrs, CT, USA

⁵Department of Earth and Atmospheric Sciences, University of Houston, Houston, TX, USA

⁶Institute of Archaeology and Ethnography, National Academy of Sciences of the Republic of Armenia, Yerevan, Armenia

⁷Department of Earth Sciences, Royal Holloway, University of London, UK

⁸NERC Argon Isotope Facility, SUERC, East Kilbride, UK

⁹Yerevan State University, Yerevan, Armenia

¹⁰Department of Geography, Faculty of Science and Engineering, Swansea University, Swansea, UK

Received 17 May 2021; Revised 15 August 2021; Accepted 18 August 2021

ABSTRACT: The significance of the southern Caucasus in understanding Pleistocene hominin expansions is well established. However, the palaeoenvironments in which Palaeolithic occupation of the region took place are presently poorly defined. The Hrazdan river valley, Armenian Highlands, contains a rich Palaeolithic record alongside Middle Pleistocene volcanic, fluvial and lacustrine strata, and thus offer exciting potential for palaeoenvironmental reconstruction. We present the first results of sedimentological, geochemical, tephrostratigraphical and biological (diatoms) study of the sequence of Bird Farm 1, located in the central part of the valley. These data show six phases of landscape development during the interval 440–200 ka. The sequence represents the first quantitative Pleistocene diatom record from the Armenian Highlands and the southern Caucasus, and indicates the persistence of a deep, stratified lacustrine system, with evidence for changing lake productivity that is tentatively linked to climate. Furthermore, major element chemical characterization of visible and crypto-tephra horizons in the sequence enables the first stages of the development of a regional tephrostratigraphy. Together, the evidence from Bird Farm 1 demonstrates the importance of lacustrine archives in the region for palaeoenvironmental reconstruction and highlights the potential for linkages between archives on both a local and regional scale. Copyright © 2021 John Wiley & Sons, Ltd.

KEYWORDS: Armenian Highlands; diatom analysis; palaeoenvironments; sedimentology; tephrostratigraphy

Introduction

The last three decades of archaeological research have established the southern Caucasus [defined here as the area of the Caucasus ecoregion (*sensu* Bailey, 1989) lying south of the Greater Caucasus ridge] as an important region for the study of hominin evolution and expansion. Not only have hominin fossils dating to c. 1.8 Ma been found at Dmanisi, Georgia (Gabunia *et al.*, 2000; Ferring *et al.*, 2011; Lordkipanidze *et al.*, 2013), the oldest known outside Africa, but at c. 320 ka, the earliest evidence of stone tool technology and hence cognitive developments that marked the beginning of the Middle Palaeolithic are evidenced at Nor Geghi 1 (NG1), Armenia (Adler *et al.*, 2014). Furthermore, sites in the region document Neanderthal and *Homo sapiens* occupations in a range of topographic and environmental settings before, during and after the Middle to Upper Palaeolithic transition (e.g. Adler *et al.*, 2006, 2008; Bar-Yosef *et al.*, 2006; Golovanova *et al.*, 2010; Pinhasi *et al.*, 2011a, 2012; Tushabramishvili *et al.*, 2012; Gasparyan *et al.*, 2014; Moncel *et al.*, 2015; Frahm *et al.*, 2016; Pleurdeau *et al.*, 2016; Kandel *et al.*, 2017; Glaubergerman *et al.*,

2020a; Cullen *et al.*, 2021; Malinsky-Buller *et al.*, 2021). The archaeological record of the region is particularly significant given the southern Caucasus' contrasting topography, bedrock geology, climate and, hence, vegetation – factors that must have provided both constraints and opportunities for the exploitation of the area by past hominin populations. Indeed, such limitations and possibilities would have been exaggerated in the Pleistocene given the magnitude and frequency of climate change, and the intensity of regional seismicity and volcanism. Nevertheless, despite the importance that climate and environment must have played in hominin occupation of the region – for example in determining the sub-regions that could be occupied, the seasonality of activity, resources available for subsistence – few palaeoenvironmental or palaeoclimate archives have been investigated beyond the level of the individual archaeological site [e.g. palynology at Hovk 1, Armenia and Dzudzuana, Georgia (Pinhasi *et al.*, 2008, 2011b; Bar-Yosef *et al.*, 2011)]. In recent years, several studies focusing on landscape dynamics recorded by fluvial archives (e.g. Ollivier *et al.*, 2016; Suchodoletz *et al.*, 2016) and loess-palaeosol sequences (e.g. Wolf *et al.*, 2016) have allowed inferences to be made regarding glacial–interglacial palaeoenvironmental change, while palaeoclimate from some of these

*Correspondence: Jenni E. Sherriff, as above.

E-mail: jennifer.sherriff@kcl.ac.uk

sequences has been derived from the study of *n*-alkane biomarkers (Trigui *et al.*, 2019; Glauberman *et al.*, 2020b) and molluscan assemblages (Richter *et al.*, 2020). However, except for Early Pleistocene palaeobotanical remains from lacustrine sequences from the Syunik region of southern Armenia (Joannin *et al.*, 2010; Ollivier *et al.*, 2010), data of regional palaeoenvironmental and palaeoclimate relevance are only presently available from areas adjacent to the southern Caucasus, i.e. from Lake Van in eastern Turkey (e.g. Litt *et al.*, 2014; Litt and Anselmetti, 2014; Pickarski *et al.*, 2015; Pickarski and Litt, 2017) and Lake Urmia in north-west Iran (Djamali *et al.*, 2008). Given the heterogeneous geography of the area, it is debatable how far these Turkish and Iranian records are applicable to the southern Caucasus.

The Hrazdan valley, in central Armenia, has been a particular focus of Pleistocene geoarchaeological research, in part because its Palaeolithic record has been well documented since the Soviet era (see Gasparyan *et al.*, 2014). In the central part of the valley the river has incised a gorge that exposes volcanic, fluvial and lacustrine strata. This suite of deposits is a product of the flow of mafic lavas along the valley from sources in the Aragats and Gegham volcanic massifs during the Early and Middle Pleistocene, respectively. These lavas dammed the river leading to the formation of lakes in their lea, while subsequent downcutting of the River Hrazdan led to the breach of the dams and deposition of alluvium in the newly formed floodplain (Sherriff *et al.*, 2019). A series of such volcanic–lacustrine–alluvial phases have been identified and dated from before c. 440 to c. 200 ka. Indeed, the association of terrigenous sediment, archaeological material and volcanic strata offers the possibility of preservation of palaeoenvironmental and palaeoclimate proxies in lacustrine deposits, precise dating of the archaeological and geological record by $^{40}\text{Ar}/^{39}\text{Ar}$, and tephrostratigraphic correlation between sites and sequences (Sherriff *et al.*, 2019). Key among the sites demonstrating such potential is NG1, a locale from which >15 000 obsidian artefacts were recovered during excavations in 2008–2017, and which document the change from Lower to

Middle Palaeolithic technologies (Adler *et al.*, 2014; Frahm *et al.*, 2020). NG1 is associated with alluvium and multiple palaeosols lying beneath both the youngest lava in the Hrazdan gorge (HGW-VI of Sherriff *et al.*, 2019) and an underlying tephra $^{40}\text{Ar}/^{39}\text{Ar}$ dated to c. 308 ka (Adler *et al.*, 2014), but biological proxies have not been preserved. However, a fossiliferous lacustrine and fluvial sequence beneath the same upper lava as found at NG1 exposure is located 1.35 km to the south-west of NG1 at ‘Bird Farm 1’ (BF1). Here we report combined litho-, bio-, tephro- and chronostratigraphic data from BF1. Our aims in so doing are to (i) develop a model of climate and landscape change in the Hrazdan valley, (ii) provide palaeoenvironmental context for hominin occupation at NG1 and (iii) demonstrate the applicability of fragmentary lacustrine archives for improving our understanding of Middle Pleistocene environmental change in the Armenian Highlands and broader Caucasus region.

Geological and site context

BF1 (40°20'9.4"N, 44°34'53.1"E, 1388 m asl) is located c. 17 km north of Yerevan and is situated on the western side of the Hrazdan gorge, in the north-eastern Armenian Highlands (Fig. 1). The surrounding mountains of the Gegham range reach elevations of 2304 m asl (Mt. Gutansar, 9.3 km north-east of BF1) and 2506 m asl (Mt. Hatis, 12.5 km east), while 14 km west of BF1, Mt. Arailer rises to 2604 m asl (Karapetyan and Adamyan, 1973). The large altitudinal variations mean that although characterized by a continental climate regime, average annual temperatures range from -4°C to $+21^{\circ}\text{C}$, while there is a mean 400 mm of annual rainfall (Acopian Centre for the Environment, 2019).

The Armenian Highlands and the Caucasus (Greater and Lesser) mountain ranges mark the juncture of the Near East and Eurasia. Covering an area over 300 000 km², the Armenian Highlands is the southernmost of the mountain chains and

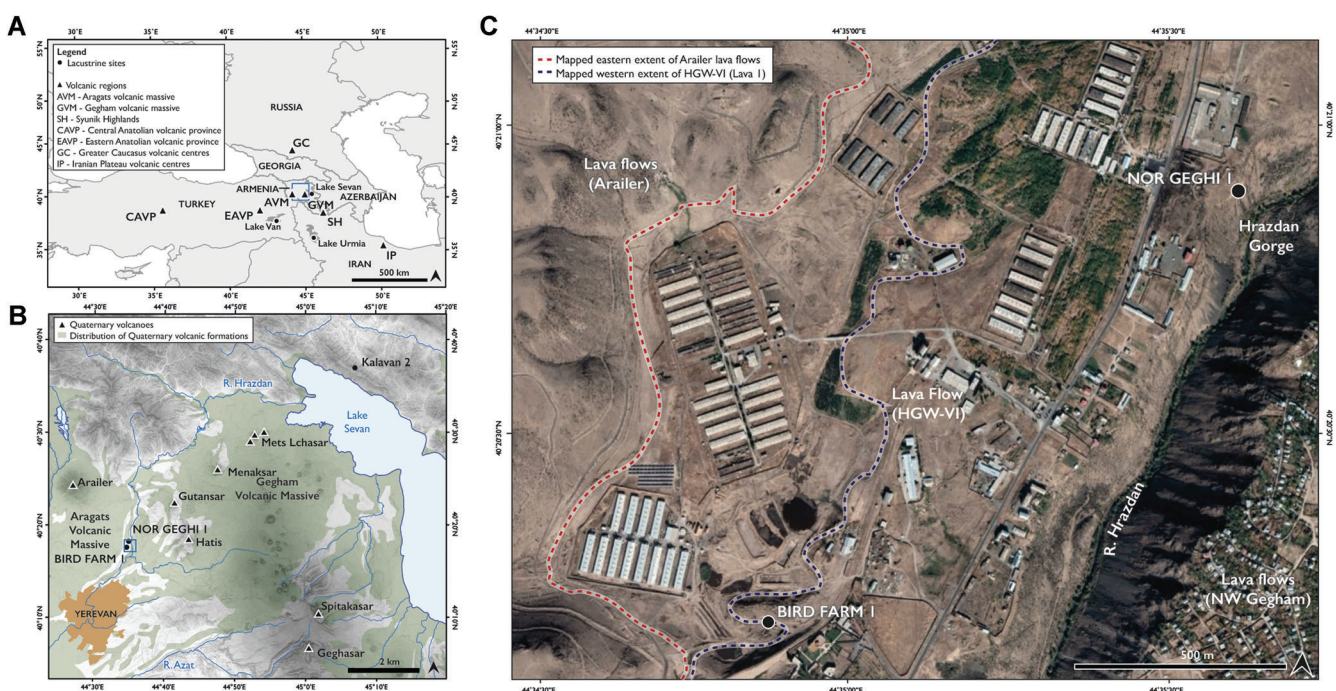


Figure 1. Location map. (A) Regional map showing location of the southern Caucasus (as defined by Bailey, 1989) and positions of main volcanic regions and major lakes in the region. Blue box represents the location of B. (B) Map of the Hrazdan basin. Extent of the Quaternary volcanic deposits and main volcanic centres are highlighted. Blue box represents the location of C. (C) Satellite image showing the locations of BF1 and NG1 (imagery from Google Earth, 2021).

borders the Iranian Plateau to the east, the Anatolian Plateau to the west and the Mesopotamian Plain to the south (Abich, 1845), while at its northern margin, the Armenia Highlands merge with the Lesser Caucasus. Both ranges were formed because of continental collision of the Arabian and Eurasian plates from the Miocene onwards (Sosson *et al.*, 2010). This tectonic activity also caused significant volcanic activity during the late Neogene and Quaternary, forming a range of volcanic landforms and strata which are clearly expressed across the region today (Sherriff *et al.*, 2019; Halama *et al.*, 2020, and references therein). BF1 lies within the NW margin of the Gegham volcanic massive (GVM) and close to the eastern margin of the Aragats volcanic massive (AVM). Locally, the AVM is represented by the Mt. Arailer stratovolcano, while Gutansar, Hatis and Mensakar, together with smaller features at Alapars (12.5 km north-west of BF1) and Fantan (11 km north-west), are the main volcanic centres of the western part of the GVM. Together, the edifices and associated volcanic deposits of Gutansar, Alapars and Fantan form the Gutansar Volcanic Complex (GVC).

The AVM and GVM are separated by the River Hrazdan, which flows NE–SW from Lake Sevan across the Hrazdan–Kotayk Plateau before draining into the River Araxes 18 km south of Yerevan. BF1 lies c. 0.6 km to west of the Hrazdan river and coincides with a lava plateau representing the western margin of the GVM. Lava flows emanating from Arailer terminate c. 0.7 km to the west of the site and at a 50 m higher elevation. The mode and chronology of GVM and AVM volcanism have been described in detail elsewhere (Lebedev *et al.*, 2011, 2013; Sherriff *et al.*, 2019; Gevorgyan *et al.*, 2020) and are only briefly reviewed here.

Previously published stratigraphies and chronologies of lava flows and pyroclastic deposits in the Hrazdan valley indicate that the area was subjected to several phases of volcanism during the Early and Middle Pleistocene. The earliest phase is associated with Arailer and the AVM between 1.40 and 0.65 Ma based on K–Ar and $^{40}\text{Ar}/^{39}\text{Ar}$ dating of lava flows and pyroclastic deposits near the Arailer edifice (Lebedev *et al.*, 2011; Gevorgyan *et al.*, 2020). A combination of K–Ar, $^{40}\text{Ar}/^{39}\text{Ar}$ and fission track (FT) dating of volcanic formations associated with the NW sector of the GVM indicates a least four phases of volcanic activity between 700 and 200 ka (Karapetian *et al.*, 2001; Lebedev *et al.*, 2013; Sherriff *et al.*, 2019). After 200 ka, the Hrazdan incised through

the Lower–Middle Pleistocene volcanic strata, producing a c. 90-m-deep gorge and exposing in section the lava flows associated with the GVM and, more rarely, sediment sequences interbedded between successive lava flows (Sherriff *et al.*, 2019). These sequences have revealed a consistent pattern of lacustrine sedimentation succeeded by alluvial activity and then floodplain soil development (Frahm *et al.*, 2017; Sherriff *et al.*, 2019). BF1 is one such sequence.

BF1 directly underlies HGW-VI (Basalt 1; Adler *et al.*, 2014; Sherriff *et al.*, 2019), which is one of the youngest lava flows exposed in the Hrazdan gorge. This lava has a clear surface expression and is traceable along the western side of the Hrazdan valley, where it directly overlies HGW-IV (Fig. 1), while chronological data for both lavas have been published from NG1 (Adler *et al.*, 2014). Here a series of alluvial sediments incorporating several phases of pedogenesis are interbedded between HGW-IV and HGW-VI, while $^{40}\text{Ar}/^{39}\text{Ar}$ dating has produced ages of 441 ± 6 and 197 ± 7 ka for HGW-IV and HGW-VI, respectively. $^{40}\text{Ar}/^{39}\text{Ar}$ dating of a volcanic ash unit in the uppermost stratum of the NG1 sequence (Unit 1) yielded an age of 308 ± 3 ka (Adler *et al.*, 2014). Although HGW-IV is not visible in the locality of BF1, it is likely that BF1 and NG1 are at least broadly contemporary given (i) a similar association with HGW-VI, (ii) both contain a comparable alluvial sequence overlying a lacustrine deposits (see below), and (iii) the two sites have a similar outcrop elevation (1402 m asl at NG1 and 1388 m asl at BF1).

Materials and methods

Fieldwork

The BF1 exposure was initially identified during a 2009 geomorphological survey. It comprises a 9 m high and 100 m long upstanding section exposed in the northern wall of a ‘borrow pit’ and is located immediately south of a chicken rearing facility (hence our ‘Bird Farm’ name for the site – the locale has no local toponym). The site has been revisited on several occasions (2011, 2013, 2015, 2017 and 2018) to excavate a test pit through to the base of the sequence, clean and describe the section, construct a formal log, and to sample the sequence for biostratigraphic and chronometric studies (Fig. 2). The analyses reported below were carried out on contiguous 2-cm-thick blocks of sediment taken through

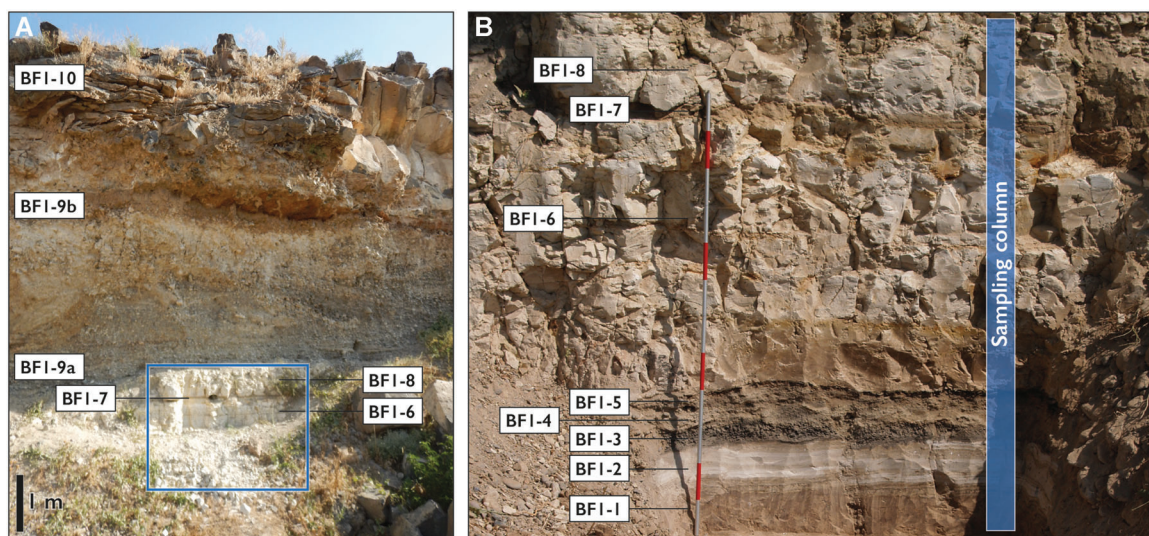


Figure 2. Site photographs. (A) Overview of the BF1 section. Blue box indicates the position of B. (B) Detail of BF1-1 to BF1-8. Shown is the location of the contiguous sampling column for sedimentology, geochemistry, diatom analysis and tephrostratigraphy. Positions of micromorphology samples are shown in Fig. 3.

fine-grained strata and micromorphological study was conducted on 12 monolith samples collected in 120 × 60 mm stainless steel tins.

Bulk sedimentology, micromorphology and sediment geochemistry

Before laboratory analysis, the sediment subsamples were divided for separate bulk sedimentology/geochemical and tephrostratigraphic analyses. The sedimentology fraction was oven dried at 40°C and then disaggregated. The dried samples were sieved at 2 mm and the <2 mm fraction was retained for bulk sedimentological and geochemical analysis.

Mass-specific magnetic susceptibility (MS) was determined using a Bartington MS2 meter with MS2c dual frequency sensor at low (0.46 kHz) frequency (X^{lf}) following the protocol outlined by Dearing (1999). Percentage organic content (%OC) and calcium carbonate content (%CaCO₃) were estimated from loss-on-ignition at 550 and 1000°C, respectively (Heiri *et al.*, 2001). %CaCO₃ values were very low throughout the sequence (<2 %) and so are not considered further. Particle size analysis (PSA) was undertaken using a Malvern Mastersizer 3000 laser granulometer with a Hydro UM accessory following the protocol described by Glauberman *et al.* (2020b).

Micromorphology samples were prepared using standard impregnation techniques developed in the Centre for Micromorphology at Royal Holloway, University of London (Palmer *et al.*, 2008). Thin sections were analysed using an Olympus BX-50 microscope with magnifications from 20× to 200× and photomicrographs were captured with a Pixera Penguin 600es camera. Thin section description followed terminology outlined in Bullock *et al.* (1985) and Stoops *et al.* (2018).

Major and trace elemental concentrations of the <2 mm bulk sediment samples were measured using a Thermo Scientific Niton XL3 portable X-ray fluorescence analyser (pXRF) using the approach outlined by Glauberman *et al.* (2020b). The pXRF data in this study are used semi-quantitatively; however, note that several studies have demonstrated that measured elemental concentrations of bulk sediment samples using pXRF closely correspond to elemental concentrations derived from conventional XRF analysis (Roy *et al.*, 2012, 2013).

Tephrostratigraphy

Sediment subsamples from the BF1 sequence were prepared for crypto-tephrostratigraphic analysis following standard density separation procedures (e.g. Blockley *et al.*, 2015) and peaks in glass shard concentration were quantified following Gehrels *et al.* (2008), using *Lycopodium* spiking to aid counting of high shard concentrations. Peaks in glass shard concentration were subsequently prepared for major and minor element chemical characterization using density separation, but with the omission of the combustion stage to avoid thermal alteration (Pilcher and Hall, 1992; Van den Bogaard and Schmincke, 2002). Individual volcanic glass shards were hand-picked onto silicon sheets and impregnated in an epoxy resin ready for chemical analysis (see Hall and Hayward, 2014). In addition to the sediment samples, three visible tephra layers identified in the BF1 sequence (BF1-3, BF1-5 and BF1-7) were sampled as part of the contiguous sampling column and prepared following the methodology outlined above. Owing to the thickness and composition of BF1-3, a larger bulk sample from the unit was taken in addition to those from the sediment sampling column. This was processed by wet sieving a subsample of c. 2 g⁻¹ through 250- and 125-µm meshes. The

intermediary fraction was retained and prepared for chemical analysis in the same manner as the other glass shard samples.

Chemical analysis was undertaken on the three visible tephra layers identified in the field [BF1-3 (BF 142–144), BF1-5 (BF 122–124 and BF 124–126), BF1-7 (BF 46–48)] and on six peaks in glass shard concentrations as determined from the cryptotephra investigation (BF 154–156, BF 146–148, BF 116–118, BF 112–114, BF 104–106, BF 82–84) (Fig. 3). Resin stubs containing cryptotephra and visible ashes were carbon coated and analysed for major and minor elements using the WDS-EPMA (Cameca SX-100) facility at the University of Edinburgh. Probe conditions were guided by Hayward (2012). Calibration, precision and drift were assessed by the analysis of internal Lipari and BCR-2G secondary standards (Supporting Information 1).

Diatom analysis

Thirty-one sub-samples were prepared for diatom analyses from units BF1-6, BF1-7 and BF1-8 following the digestion procedure of Battarbee *et al.* (2001). Samples were studied at a magnification of 1000× using a Lecia DMBL. Identifications followed Krammer and Lange-Bertalot (1986, 1988, 1991a, b), supplemented with Lange-Bertalot (2001) and Krammer (2002) and were complemented by web-based resources (Spaulding *et al.*, 2020) and Algaebase (Guiry and Guiry, 2018).

Stratigraphy, sedimentology and geochemistry

Site stratigraphy

Ten stratigraphic units (BF1-1 to BF1-10) were identified in the BF1 sequence (Fig. 3; Table 1). Evident in the sequence is a mixture of volcanic (BF1-3, BF1-5, BF1-7, BF1-10), volcanoclastic (BF1-2, BF1-4) and siliciclastic (BF1-6, BF1-8, BF1-9a-b) deposits while there is also evidence of the development of at least one palaeosol within BF1-9 (BF1-9b).

The lowermost unit (BF1-1) comprises massive poorly sorted sand-silt, but its base lies beneath the borrow pit floor and could not be found in the 2011 test pit. BF1-1 is overlain by horizontally laminated medium sand-silt and sand-silt-sized volcanic ash (BF1-2), which in turn is capped by massive, granular scoria lapilli (BF1-3). The overlying stratum comprises horizontally bedded coarse-fine sand with occasional granule-grade scoria lapilli (BF1-4), which in turn is capped by normally graded granule to coarse silt-grade scoria lapilli and ash (BF1-5). There is a sharp contact between BF1-5 and BF1-6, while the latter consists of well-sorted massive-laminated medium silt. BF1-6 is overlain by a massive, well-sorted very coarse silt-sized volcanic ash (BF1-7) which in turn is capped by a well-sorted massive-laminated medium silt (BF1-8). An unconformity represented by a sharp, undulating contact separates the fine-grained sequence outlined above from predominantly coarse-grained clastic sediments. These are represented first in BF1-9a, which comprises matrix-supported, trough cross- and planar-bedded, gravels of subrounded-rounded pebble- and cobble-sized clasts in a coarse sand matrix. Within this unit are lenticular beds of laminated granules-coarse sands, and clasts are primarily of mafic lava, with lower frequencies of obsidian, intrusive igneous, metamorphic and sedimentary lithologies (Table 1). Also present within BF1-9 are intraclasts consisting of material derived from BF1-6 and/or BF1-8. BF1-9b conformably overlies BF1-9a and comprises clast- and matrix-supported gravels as described for the latter. However, the matrix of BF1-9b exhibits normal grading from coarse sand to sandy clay

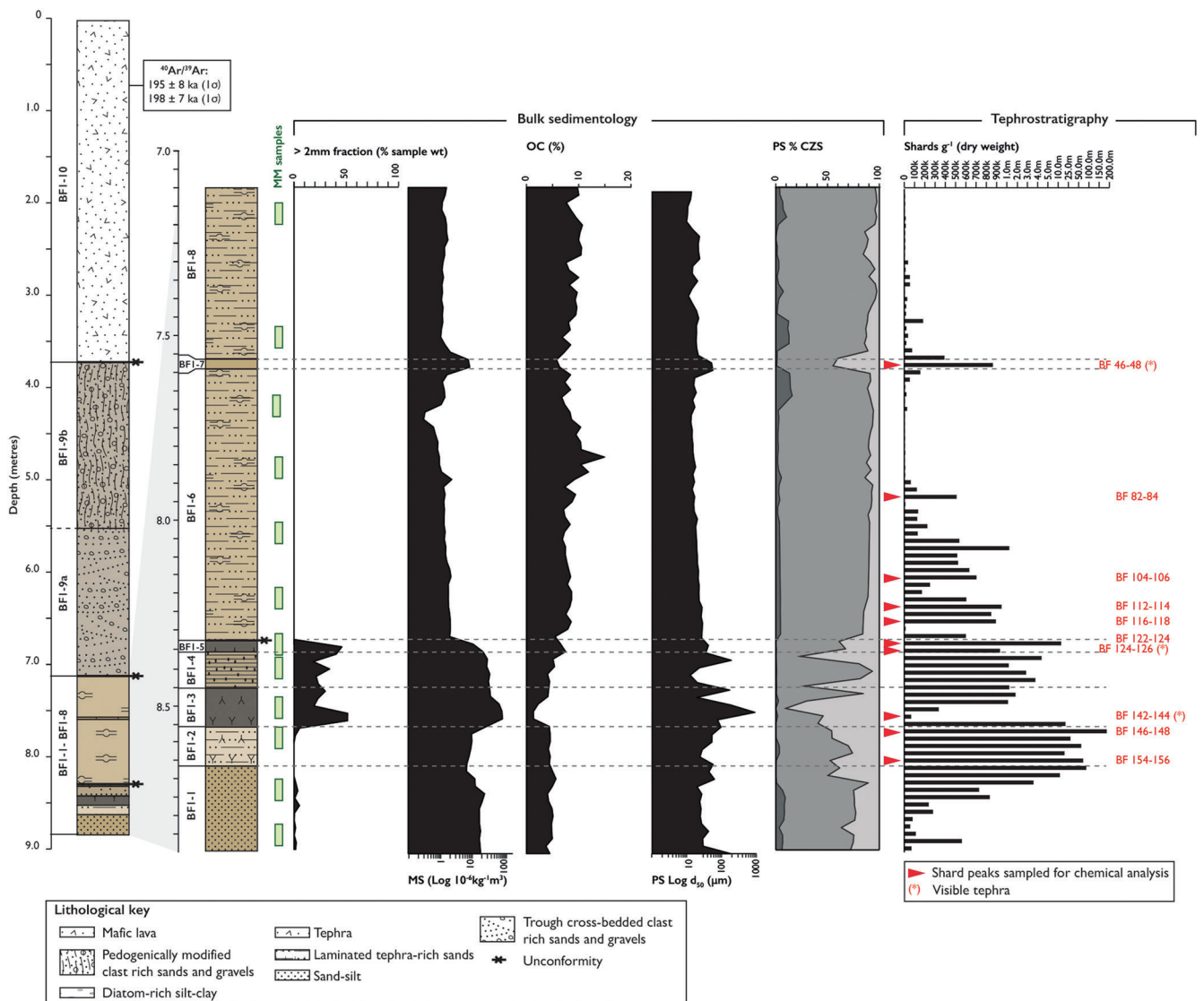


Figure 3. Summary of bulk sedimentology and tephrostratigraphy of BF1-1 to BF1-8. Shown are %>2 mm fraction, low-frequency mass-specific magnetic susceptibility (on \log_{10} scale), median particle size (D_{50} μm on \log_{10} scale) and %clay (dark grey), %silt (medium grey) and %sand (light grey). Positions of micromorphological samples (MM) are also shown. Glass shard counts are shown per g/dry weight. Red arrows and text represent levels selected for geochemical analysis.

and is also formed of sub-angular aggregates with Fe/Mn oxide coatings and carbonate rhizoliths. Stage III carbonate coatings (*sensu* Gile, 1961) are present on gravel clasts. The BF1 sequence outlined above is capped by mafic lava (BF1-10) which thins to the east of the BF1 outcrop. BF1-10 has a blocky structure and rubbly base, while its upper surface is weathered and has developed a stage III carbonate crust. BF1-10 represents the local outcrop of HGW-VI in the Hrazdan valley stratigraphy and has been dated by $^{40}\text{Ar}/^{39}\text{Ar}$ at BF1 to 195 ± 8 and 198 ± 7 ka (Sherriff *et al.*, 2019).

Bulk sedimentology

The results of the bulk sedimentological analyses undertaken on the <2 mm sediment size fraction indicate that the BF1-1 to BF1-8 deposits are moderately to poorly sorted and range in grain size from fine silt to very fine sand (Fig. 4). X^{lf} values range from 0.34 to $94.69 \times 10^{-6} \text{ kg}^{-1} \text{ m}^3$ through the sequence, while organic carbon content (%OC) is low (<15%). However, there are clear trends in particle size distribution, X^{lf} and organic carbon content both between, but also within stratigraphic units (%OC,

Fig. 3). BF1-1 has a moderately sorted medium silt grain size, low %OC and a relatively high X^{lf} . BF1-2 is characterized by lower X^{lf} compared to BF1-1, a low %OC and a slightly coarser grain size than the underlying unit. A shift to higher X^{lf} than that seen in BF1-1 and BF1-2 characterize BF1-3 to BF1-5, while these strata are also characterized by low %OC. Variation in particle size distribution is evident through BF1-3 to BF1-5, with the <2-mm fraction of BF1-3 principally comprising medium sand to granular ash and lapilli, while BF1-4 and BF1-5 are principally composed of coarse silt to very fine sand particles. A clear shift in all sedimentological parameters is observed at the BF1-5 to BF1-6 boundary, with BF1-6 characterized by relatively high %OC, low X^{lf} values and a generally finer particle size distribution than the underlying strata. There is also an observable increase in %OC in BF1-6 through the interval 7.92–7.62 m accompanied by a decrease in X^{lf} . BF1-7 marks a return to relatively high X^{lf} and low %OC, while grain size parameters indicate that the unit is a well-sorted very coarse silt. BF1-9 has comparable sedimentological properties to BF1-6, with elevated %OC, low X^{lf} and a fine-medium silt grain size.

Table 1. Summary of BF1 stratigraphic units.

Unit	Depth (metres from top of sequence)	Field description	Micromorphological observations*	Depositional environment
BF1-10	0.00–3.70	Weathered mafic lava comprising sphere and sphere-like boulder sized clasts. Base of unit is characterized by a bubbly base and sharp/truncated contact with unit 2. Thin crust of carbonate over the exposed surface of a lava, forming a thin white crust. Unit thins to the east of section		Mafic lava flow (HGW-VI, Sherriff <i>et al.</i> , 2019)
BF1-9b	3.70–4.80	Clast- and matrix-supported gravels comprising sub-rounded to rounded clasts of diverse lithologies [mafic lava, granite (Cambrian), marble, obsidian (from felsic lavas/pyroclastic deposits?), perlite and diatomite]. Matrix comprising pedogenically modified sand/silt with Fe/Mn coatings, carbonate rhizoliths. Stage III carbonate coating around clasts. Matrix grain size fines upwards from sand to sandy clay. Sharp (forming channel scour in east side of section) to: Clast- and matrix-supported gravel of rounded and sub-rounded basalt, granite (Cambrian), marble, obsidian (from acid lavas), perlite and diatomite clasts in coarse sand matrix. In basal 1 m forming trough cross-bedded features with lenticular beds of laminated 10YR 7/2 coarse sands and coarse sand/granules. Upper part of bed formed of planar sheet structures of 0.5–0.3-m-thick sets of pebbles-coarse sands and cobble/pebbles.		Pedogenically modified fluvial gravels forming compound Bk1, Bk2, Bk3, Bck, Ck horizons (Inceptisol)
BF1-9a	4.80–7.10			Moderate-energy fluvial gravels representing lateral accretion of channel and bedforms
BF1-8	7.10–7.56	2.5 Y 8/4 (dry), 2.5 Y 7/4 (wet) massive-laminated clay with frequent dark trace fossils of grassy plant remains. Shears along lamina planes. Well sorted. Sharp boundary to:	Massive-weakly, matrix-supported structure; c/f ratio between 1: 2 (ranging from few to frequent); grain common [quartz (rounded), feldspar (rounded)], mafic lithic fragments and volcanic ash; matrix of silt-clay; frequent to common diatoms (pennate, centric, acicular), few amorphous algal mats, few amorphous organic fragments. Fe/Mn mottling of matrix.	Low-energy deep-water lacustrine
BF1-7	7.56–7.60	2.5 Y 7/4 (dry), 2.5 Y 6/4 (wet) well-sorted fine sand-sized ash laid down in coarse, straight, continuous, parallel laminae. Well sorted. Sharp boundary to:		Primary tephra fall
BF1-6	7.60–8.32	2.5 Y 8/4 (dry), 2.5 Y 7/4 (wet) laminated clay with frequent dark trace fossils of grassy plant remains. Shears along lamina planes. Well sorted. Sharp boundary to:	Massive-weakly horizontally laminated, matrix-supported structure; c/f ratio between 1: 3 and 1: 4. Laminae have diffuse contacts and characterized by variation in abundance of grains (ranging from few to frequent); grain lithologies of quartz (rounded), feldspar (rounded), mafic lithic fragments and volcanic ash; matrix of silt-clay; frequent to dominant diatoms (pennate, centric, acicular), few amorphous algal mats, few amorphous organic fragments.	Deep-water lacustrine
BF1-5	8.32–8.36	2.5 Y 3/1 (dry) Pumice of angular to sub-angular fine pebble-sized structures. Sharp boundary to:	Normally graded grain-supported structure; c/f ratio of 9: 10; grains exclusively igneous lithologies (scoria, mafic lithic fragments, volcanic glass; mineral grains including plagioclase, biotite, olivine); matrix of volcanic ash. Upper strata characterized by random-stipple striated b-fabric and increased frequency of clay in matrix; clay hypocoating of	Primary tephra fall

(Continued)

Table 1. (Continued)

Unit	Depth (metres from top of sequence)	Field description	Micromorphological observations*	Depositional environment
BF1-4	8.36–8.48	2.5 Y 6/3 massively bedded medium sand with occasional granular and pebble-sized angular and sub-angular pumice clasts. Moderately sorted. Sharp boundary to:	grains; clay infillings of pumice/scoria vacuoles. Bedded microstructure. Lamination thickness of 50–200 mm, c/f ratio ranges from 1: 2 to 4: 1; beds massive with diffuse boundaries. Dominant grains [mafic lithic fragments, volcanic glass, mineral grains (including plagioclase, biotite, feldspar, quartz, olivine)]; matrix of fine silt and ash. Frequent elongate amorphous organic material; few diatom frustules (centric and pennate).	Shallow-water lacustrine
BF1-3	8.48–8.58	2.5 Y 3/1 pumice gravel of sub-angular to angular granular and fine pebble-sized clasts in coarse sand matrix. Moderately sorted (sampled for tephra). Sharp boundary to:	Massive grain-supported structure; c/f ratio of 9: 10; grains exclusively igneous lithologies (scoria, mafic lithic fragments, volcanic glass; mineral grains including plagioclase, biotite, olivine); matrix of volcanic ash. Rare Fe/Mn mottling of matrix.	Primary tephra fall
BF1-2	8.58–8.68	2.5 Y 8/4 (dry), 2.5 Y 7/4 (wet) massive–laminated silty clay. Sharp-graded contact to:	Laminated microstructure. Lamination thickness of 300–750 mm, c/f ratio ranges from 3: 7 to 9: 10; Laminations massive or normally graded with sharp boundaries. Dominant grains [mafic/felsic lithic fragments, pumice, scoria volcanic glass, mineral grains (including plagioclase, biotite, feldspar, quartz, olivine)]; matrix of fine silt and ash. Fe/Mn spherules frequent; rare amorphous organic material. Fe/Mn enrichment of matrix at contact with BF1-3.	Volcanoclastic. Shallow-water lacustrine with reworked ash fall
BF1-1	8.68–8.80	Well-sorted massive silty sand.	Massive microstructure; c/f ratio of 1: 1; common grains (mafic/felsic lithic fragments, volcanic glass, mineral grains (including plagioclase, biotite, feldspar, quartz). Lithic fragments have peculiar alteration; matrix of fine silt and ash; Fe/Mn mottling of matrix and hypocoating of grains and void; rare amorphous organic material and angular organic fragments.	Shallow-water lacustrine

*Very dominant = >70% of slide cover, dominant = 50–70%, common = 30–50%, frequent = 15–30%, few = 5–15%, very few = <5%.

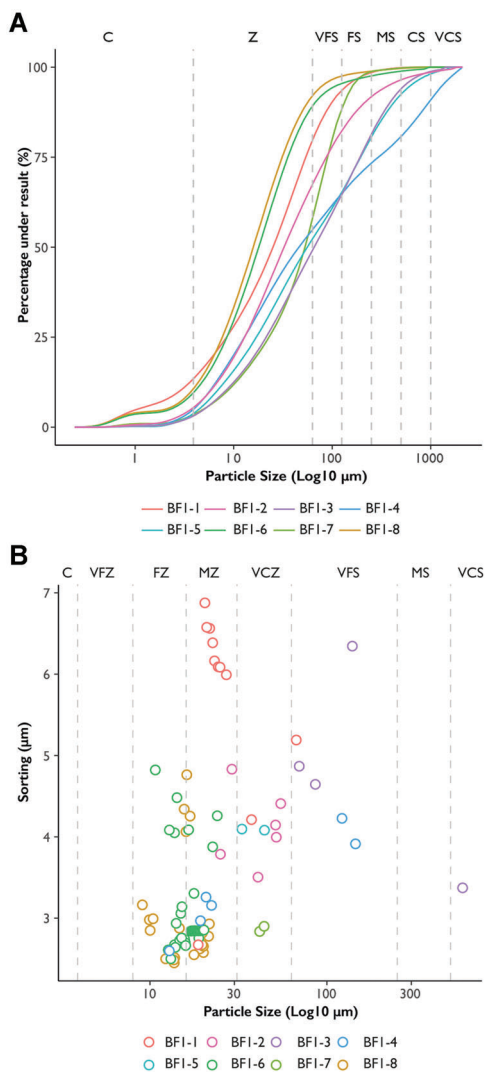


Figure 4. Particle size distribution of BF1- to BF1-8. (A) Cumulative frequency distribution for average particle size for each unit. (B) XY plot showing mean particle size against sorting (calculated following method of Folk and Ward, 1957).

Thin section micromorphology

The main micromorphological properties of the BF1 deposits are presented in Table 1. Overall, the sequence is characterized by a high abundance of volcanic and siliclastic mineral fractions, with variations in the lithological and microstructural properties of these fractions evident between individual units.

At the microscale, BF1-1 has a massive microstructure, with equal proportions of fine silt and volcanic ash matrix (Fig. 5A). Mafic/felsic lithic fragments and feldspar mineral grains are present, while Fe/Mn oxide mottling of the matrix and Fe/Mn hypocoatings of voids are common. BF1-2 comprises grain- and matrix-supported, grain-rich, normally graded laminae with sharp upper and lower boundaries (Fig. 5B). The matrix is principally of volcanic ash with some silt-grade clastic material, while grains are principally of volcanic lithologies. A loaded contact and enrichment of the matrix with clay is evident at the contact with BF1-3 (Fig. 5C) and then the latter is characterized by a massive, grain-supported microstructure. Grains are exclusively of volcanic lithologies and comprise coarse silt to granular-sized scoria fragments, many of which have Fe/Mn hypocoatings. The same high frequency of volcanic material is observable at the microscale in the overlying BF1-4. This latter unit comprises alternations at

irregular thicknesses of grain- and matrix-rich silt-sand particles with frequent volcanic ash and outsized mafic lithic fragments (Fig. 5D). Evident in the matrix are centric and pennate diatom frustules and amorphous organic material. BF1-5 has comparable textural and lithological properties to BF1-3 at the microscale, but evident towards the top of the former stratum is an increased abundance of clay in the micromorphology samples. This is expressed as the occurrence of stipple-striated β -fabric and clay coatings around grains (Fig. 5E). The upper boundary of BF1-5 is sharp and loaded, and also characterized by a high abundance of clay, with a clay-rich matrix and clear horizontal parallel β -fabric. Clay infillings of scoria vesicles are also evident. Associated with the upper part of BF1-5 are frequent occurrences of organic matter (Fig. 5F). This is represented by elongate fragments of organic material which are generally orientated sub-parallel to the unit bounding surface. Many fragments are Fe/Mn mottled.

A clear change in lithological components is recorded in the BF1-6 micromorphology samples. At the microscale, volcanic material is rare. The unit has a massive to weakly matrix rich microstructure comprising fine-medium silt-grade siliclastic material. Laminations are diffuse and represent irregular alternations of massive matrix-rich fine and medium silt. Mineral grains are rare and comprise medium silt-sized rounded quartz and feldspar (Fig. 5G). Evident in the matrix are abundant diatom frustules which are a mixture of pennate, centric and acicular forms (Fig. 5H). Also evident are amorphous algal filaments and organic fragments. Microstructural properties similar to BF1-6 are observed through BF1-8, albeit that the latter stratum is more grain-rich than BF1-6, while Fe/Mn mottling of the matrix is evident towards the top of BF1-8.

Bulk sediment geochemistry

Figure 6 presents principal components analysis (PCA) results for selected major and minor elements (Al, Si, P, S, K, Ca, Ti, Fe, V, Cr, Zn, Rb, Sr, Zr and Ba) in BF1-1 to BF1-8. PC1 represents 38.1% of variation in the bulk geochemical data, whilst PC2 accounts for 23.4%. Evident in the PCA are differential clustering of elements, while these are presented against select bulk sedimentological parameters (X^{lf} , %OC, and D_{50} PSA) in Fig. 6A. Four groups of elements and sedimentological properties are identifiable: (i) Group A, characterized by high values of Si and %OC, (ii) Group B, identified by high K, Rb and Nb values, (iii) Group C, characterized by high values of V, Zr, Cr, Fe and Ti, and (iv) Group D, defined by Al, Sr, Ca, Zr and Ba and associated with high X^{lf} and D_{50} values.

Sample scores for PC1 and PC2 are presented in Fig. 6B, which makes clear the clustering by stratigraphic unit in this dataset. The diatom-rich strata, BF1-6 and BF1-8, plot separately from the other units and are associated with elevated Group A element concentrations, whilst BF1-2, BF1-4, BF1-5 and BF1-7 are associated with the high Group B element concentrations. BF1-1 is associated with high values of Group C elements, while the scoria-rich unit, BF1-3, is associated with both high values of Group C and Group D elements, X^{lf} and D_{50} . These trends clearly show a strong lithological control on the geochemical signature on the BF1 deposits, with the clear differentiation of units consisting of volcanic and volcanoclastic particles (BF1-2, BF1-3, BF1-4, BF1-5, BF1-7) from those composed mostly of siliclastic material (BF1-1, BF1-6, BF1-8), while there is further differentiation of the volcanic and volcanoclastic units by broad geochemical composition.

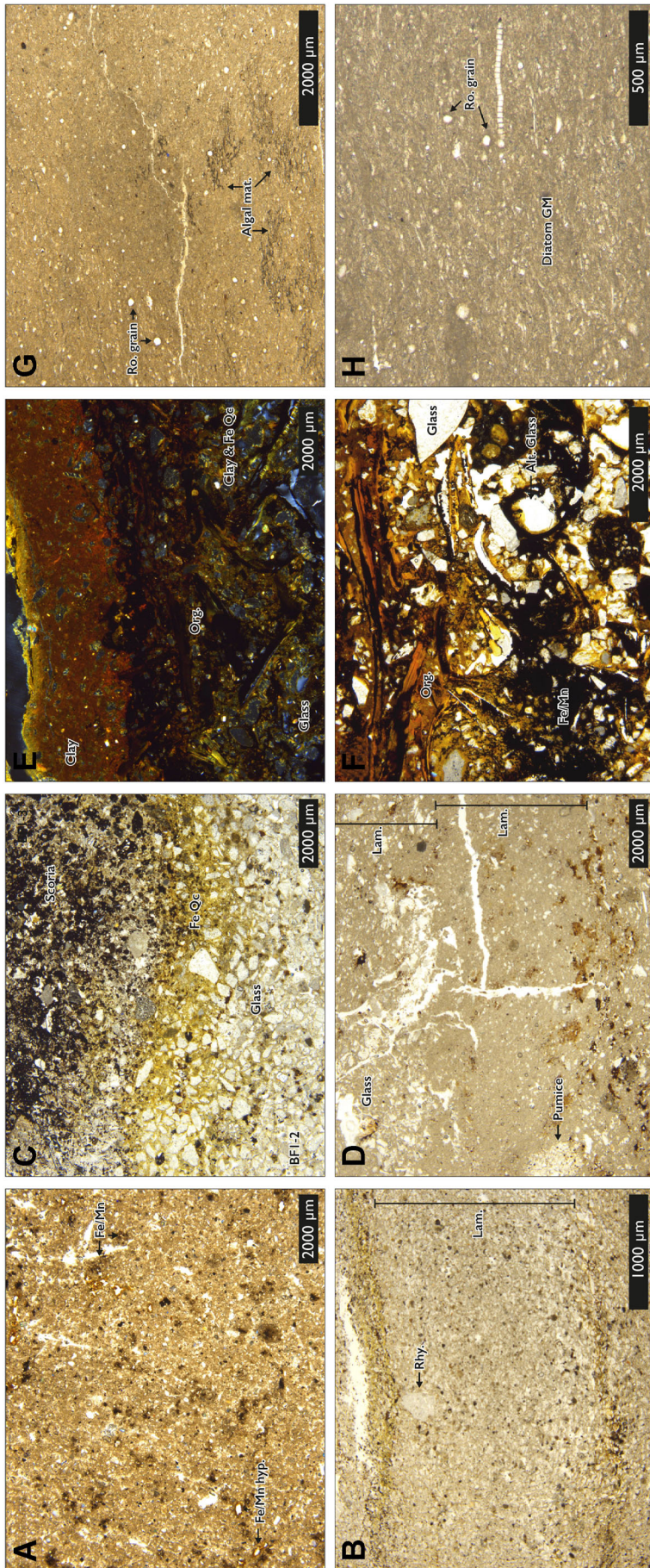


Figure 5. Photomicrographs of key micromorphological features of the BF1 sequence. (A) Massive microstructure of BF1-1 showing the presence of Fe/Mn mottling (Fe/Mn) of the groundmass and Fe/Mn hypocoatings (Fe/Mn Hyp.) of voids. Plane polarized light (PPL). (B) Laminated microstructure of BF1-2 with high volume of volcanic glass and an outsized rhyolite (Rhy.) fragment. Lam. denotes a single lamination. PPL. (C) BF1-2/ BF1-3 contact with Fe/Mn quasiccoatings (Fe Qc) around glass shards in BF1-2. A high abundance of scoria fragments is present in BF1-2. PPL. (D) Laminated microstructure of BF1-4. Lam. denotes a single lamination. Groundmass is principally volcanic glass with larger glass shards and pumice fragments present. PPL. (E) Upper surface of BF1-5. Clay and Fe quasiccoatings (Clay & Fe Qc) of volcanic material present with high abundance of clay (Clay) evident at the contact with BF1-6. Volcanic glass (Glass) and organic fragments (Org.) present. Cross-polarized light. (F) Higher magnification of BF1-4 contact showing stained organic material (Org.), altered (Alt. glass) and pristine volcanic glass and Fe/Mn mottling (Fe/Mn) of the groundmass. PPL. (G) Massive microstructure of BF1-6 showing the presence of algal material (Algal mat.) and rounded grains of quartz/feldspar (Ro. grain). Pennate, centric and acicular forms are present. Rounded grains of quartz/feldspar (Ro. grain) are also evident in the groundmass. PPL. (H) High-magnification image of BF1-8 showing diatom-rich groundmass (Diatom GM).

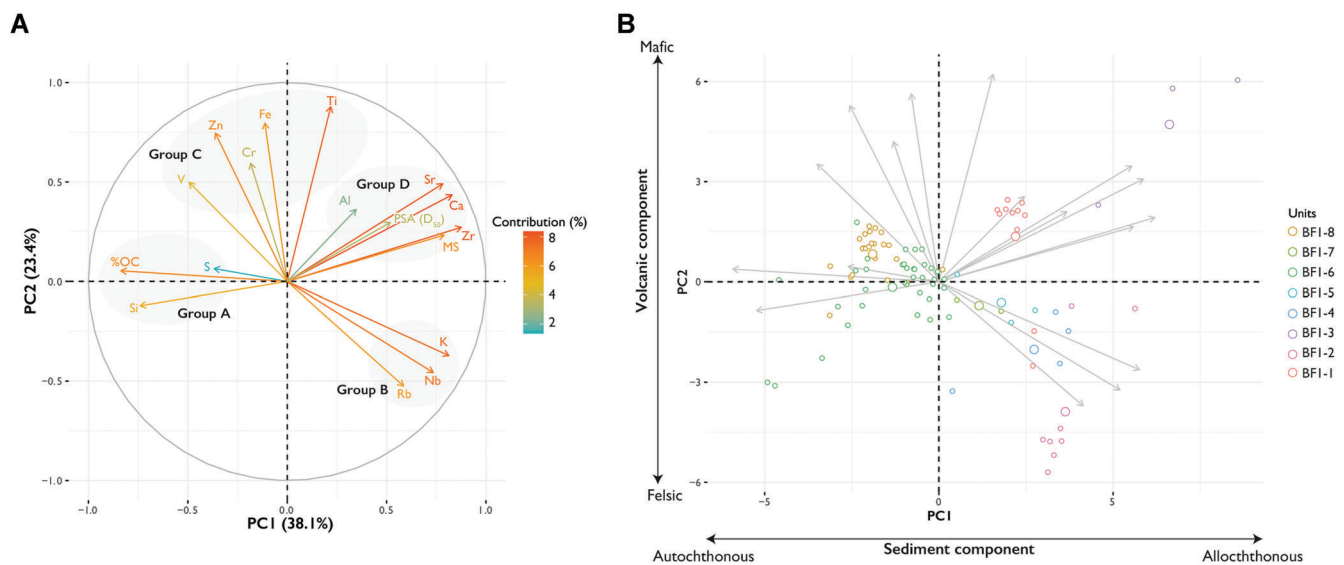


Figure 6. Summary of PCA results for the BF1 pXRF data. (A) PCA biplot of selected elemental data and sedimentological parameters. Colour coding of elements is based on their relative contribution to principal components. (B) PCA biplot of BF1 stratigraphic units.

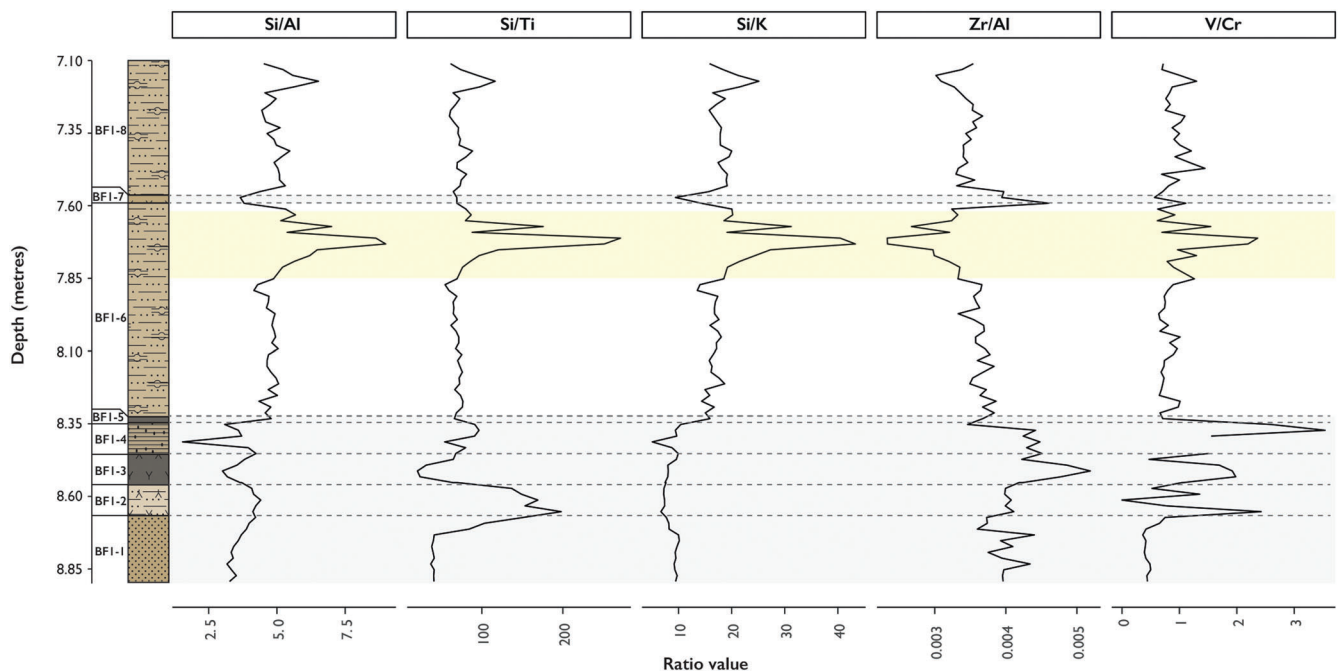


Figure 7. Ratios of selected elements (Si/Al, Si/Ti, Si/K, Zr/Al, V/Cr) through the BF1 sequence.

Si/Al, Si/Ti, Si/K, Zr/Al and V/Cr ratios are plotted against stratigraphy in Fig. 7. These ratios were selected as they give an indication of provenance (Müller *et al.*, 2001; Kylander *et al.*, 2013), the relative frequency of volcanic and siliclastic material (Martín-Puertas *et al.*, 2011; Peti *et al.*, 2020), and potential changes in biological productivity (Gill *et al.*, 2011) within a single sedimentary sequence. Si/Al shows a clear pattern of relatively low ratios in units BF1-1 to BF1-5 and BF1-7, and elevated values in BF1-6 and BF1-8. In respect of the last it is further evident that there is an increase in the Si/Al ratio in the interval 7.85–7.62-m within BF1-6. A comparable trend to that seen in Si/Al is also observed in Si/K and Si/Ti, with the exception being BF1-3, which exhibits high Si/Ti values throughout the stratum. Zr/Al shows the converse trend, i.e. elevated ratios are found in association with BF1-1 to BF1-5 and BF1-7, with lower values occurring in BF1-6 and

BF1-8. The lowest Zr/Al ratio is found in association with the interval 7.85–7.62 m. Although the dataset is characterized by a high degree of variability, especially in the lower strata, V/Cr ratios show a pattern of lower values associated with BF1-1, higher values in BF1-2 to BF1-5, and a shift back to lower values through BF1-6 to BF1-8. Elevated values of V/Cr are also recorded in the interval 7.85–7.62 m.

Sedimentological interpretation

Combined, the lithostratigraphical, bulk sedimentological, micromorphological and geochemical datasets from BF1 demonstrate clear shifts in depositional process through the sequence.

The fine and generally poorly sorted particle size distribution of BF1-1 is consistent with subaqueous sedimentation in a

shallow water setting. Impregnative Fe/Mn features representative of leaching of Fe/Mn oxides under waterlogged conditions support such an interpretation (Lindbo *et al.*, 2010). A high proportion of both siliclastic and pyroclastic relative to biological material is consistent with high allochthonous inputs into the shallow-water setting, and is reflected in the high X^{lf} (Dearing, 1999). The sedimentological properties of BF1-2 are consistent with volcanoclastic deposition, while the occurrence of laminations of principally volcanic ash probably reflect the reworking as a primary tephra fall deposit. Lower X^{lf} values in this unit compared to BF1-1 are consistent with the high proportion of felsic igneous material evident at the microscale in this unit (Dearing *et al.*, 1996). The presence of normally graded and massive laminations indicates subaqueous sediment delivery via sediment gravity flows into a shallow water body, with relative differences in particle size of the lamina reflecting variations in sediment supply and/or energy regime of these inwashing events (Stow and Bowen, 1980). The absence of significant alteration, breakage or rounding of the ash and lapilli fragments implies relatively local erosion and re-deposition of pyroclastic material.

The earliest primary tephra fall deposit in BF1 is represented by BF1-3. Elevated X^{lf} values in this unit reflect the high proportion of ferrimagnetic igneous material (scoria and mafic lithic fragments), the absence of siliclastic material and a homogeneous microstructure. The relatively coarse and poorly sorted particle size distribution of BF1-3 may imply deposition from a proximal rather than distal volcanic source (Pyle, 1989), while rapid sedimentation is suggested by load structures associated with the BF1-2 contact. A shift back to principally siliclastic sedimentation is recorded in BF1-4, where the presence of normally graded and massive laminations indicates the resumption of allochthonous sediment delivery via sediment gravity flows into a shallow lacustrine system (Lowe, 1982). The unit contains a high proportion of volcanic material, as indicated by high X^{lf} values through the unit and which is interpreted as reworking of BF1-3 tephra. The occurrence of diatom frustules in this unit indicates the first evidence of *in situ* biological productivity at BF1.

A second primary tephra fall is represented by BF1-5, while the occurrence of clay in this part of the stratum indicates that the upper surface of the tephra has been weathered (Zehetner *et al.*, 2003). Rapid *in situ* weathering and clay development is common in tephra that has been subaerially exposed (Bakker *et al.*, 1996), and is associated with the alteration of lithic fragments and fragmentation of glass shards (Sedov *et al.*, 2010). Clay enrichment in BF1-5 is therefore interpreted as representing a shift from a subaqueous to subaerial setting and subsequent exposure of the BF1-5 stratum to surface weathering processes. This conclusion is supported by the presence of organic fragments within BF1-5, which suggest that vegetation development and associated pedogenesis occurred at the former lake surface.

BF1-6 indicates the resumption of lacustrine sedimentation. Collectively, BF1-6 and BF1-8 represent the occurrence of fine-grained, diatomaceous clastic sediment deposition, while laminations indicate accretion in a deep, stratified water body. Allochthonous inputs are represented by the occurrence of silt-grade clastic particles, while variation between laminations is driven by shifts in the energy of input (Kemp, 1996). These structures are consistent with sediment delivery via sediment gravity flows, while rounded grains indicate the occurrence of some aeolian inputs (Kalińska and Nartišs, 2014). A significant autochthonous biogenic component is indicated by enhanced organic content and the abundance of diatoms. The absence of significant changes in lithological properties through BF1-6 and

BF1-8 indicates an interval of quiescent conditions that is in contrast to the underlying lacustrine strata. The only discernible changes through BF1-6 and BF1-8 are an increase in organic content and corresponding reduction in X^{lf} . These latter are interpreted as reflecting an increase in the autochthonous biogenic input associated with enhanced productivity and/or decreased catchment erosion and therefore clastic input. BF1-6 and BF1-8 are separated by the third primary volcanic unit in the BF1 sequence (BF1-7). The fine-grained and well-sorted nature of BF1-7 suggests a primary ash deposited via suspension through the lake water column.

BF1-9 is separated from the underlying strata by an unconformity, the latter marking the shift from fine- to coarse-grained clastic sedimentation. The trough and planar bedforms of the gravels and sands of BF1-9 are consistent with deposition in a moderate-energy fluvial system and probably represent lateral accretion of a braided river system (Reineck and Singh, 1980; Miall, 1996). Clast lithologies are diverse, reflecting the wide range of geological strata present in the Hrazdan valley (Kharazyan, 2005; Sherriff *et al.*, 2019). BF1-9b represents the pedogenic modification of the fluvial gravels, with the presence of carbonate and textural pedofeatures representing compound Bk1, Bk2, Bk3, Bck and Ck horizons forming within the alluvial parent material after the cessation of fluvial activity at the site. The absence of a defined A-horizon suggests that BF1-9b was truncated by the passage of the mafic lava (BF1-10) that caps the BF1 sequence.

Variations in the sedimentological properties of the BF1-1 sequence are evident in the bulk geochemistry of the deposits (Fig. 6). The clustering of strata by elemental groups (A–D) indicates a strong lithological control on the sequence. The diatomaceous units, BF1-6 and BF1-8, are found in association with elevated values of Si and high organic content (Group A), both of which are indicators of autochthonous biogenic content. Variations between elemental groups B and C probably reflect the different contributions of felsic (characterized by higher values of Rb, K and Nb) and mafic (high values of V, Zn, Fe, Cr and Ti) volcanic material in the BF1 sequence. BF1-7 and BF1-2 closely plot with Group B elements, representing a high abundance of felsic volcanic ash in these units, while the fine-grained lacustrine unit BF1-4 also plots with Group B elements, indicating the reworked volcanic component evident in thin section. The scoria-rich volcanic deposits (BF1-3 and BF1-5) are associated with elevated values of Group C elements, reflecting their mafic origin. BF1-3 and BF1-5 also occur in association with high values of Group D elements. Interpretation of a single origin of Group D is problematic, given that it contains a suite of elements associated with clastic and volcanic inputs. Nevertheless, elevated values of Group D elements in BF1-3 and BF1-5 probably reflect the elemental composition of the felsic and mafic volcanic material that comprise these units. Conversely, elevated concentrations of Group D elements in the fine-grained siliclastic unit BF1-1 are probably a product of the allochthonous inputs of detrital clastic and volcanic material within this stratum.

Lithological variations are also clearly expressed in the Si/Al, Si/Ti, Si/K, Zr/Al and V/Cr ratios (Fig. 7). Evident from these latter, however, are also changes within strata, specifically BF1-6, where an increase in Si relative to Ti, K and K is observed at 7.85–7.62 m, with an associated increase in V/Cr ratio values and decrease in Zr/Al ratio values. The interpretation of the Si profile through BF1-6 and BF1-8 is that it reflects a predominately autochthonous biogenic signal, whilst Al, K and Ti reflect contributions of detrital clastic and volcanic material. Consequently, the peak in Si relative to Al, K and Ti probably reflects either increased diatom productivity or a change in diatom composition in this interval, resulting in higher biogenic silica

loadings (Martín-Puertas *et al.*, 2011). Zr/Al ratios are frequently used for a proxy for aeolian sedimentation in lacustrine settings, given Zr is concentrated in the more mobile sand–silt fraction of clastic sediment in respect to Al (Huang *et al.*, 2003; Roy *et al.*, 2006, 2009). Although the Zr/Al relationship is complicated by the concentration of Zr in mafic volcanic minerals (Roy *et al.*, 2009, and as demonstrated by high Zr/Al ratio in BF1-3), evident in the interval 7.85–7.62 m is a decrease in Zr relative to Al in comparison to both the lower part of BF1-6 and BF1-8. This could tentatively be interpreted as a reduction in aeolian input into the lake system, occurring contemporaneously with increased biological activity. V/Cr is used as an indicator for lake anoxia, as V preferentially precipitates under anoxic conditions, whilst Cr remains relatively immobile in both anoxic and oxic settings (Schaller *et al.*, 1997; Das *et al.*, 2009). Higher V/Cr ratios values therefore may imply the persistence of anoxic conditions, possibly associated with enhanced thermal stratification or more eutrophic conditions. These shifts occur at the same interval as an increase in organic content and increased concentrations of benthic diatoms, suggesting that these geochemical signals are representative changes in lake productivity.

Tephrostratigraphy

Tephrostratigraphy results

Volcanic glass shard concentrations are high throughout the BF1 sequence, ranging from a few thousand to several million shards g^{-1} (Fig. 3; Supporting Information S1). Most of the glass shards extracted from the BF1 record are colourless, blocky and amorphous with numerous flutes and some open and closed vesicles. The surface texture on some specimens, particularly the cryptotephra, is pitted and uneven, while some specimens also exhibit cracking, all features suggestive of post-depositional alteration and hydration (Blockley *et al.*, 2005). Samples from BF1-3 comprise blocky glass shards of a distinct greenish-yellow/brown colour and rich in mineral inclusions. Alongside these were colourless shards similar to those found throughout the rest of the sequence (described above).

Tephra chemistry and correlation

Chemical classification diagrams for the visible tephra layers [BF1-3 (BF 142–144), BF1-5 (BF 122–124 and BF 124–126), BF1-7 (BF 46–48)] and peaks in glass shard concentrations as determined from the cryptotephra investigation (BF 154–156, BF 146–148, BF 116–118, BF 112–114, BF 104–106, BF 82–84) are presented in Fig. 8. The full major and minor element dataset is available and summary data are presented in Supporting Information S1. The colourless shards identified in BF1-3 (BF 142–144_b) as well as the glass shards recovered from the visible tephra BF1-5 (BF 122–124_a and BF 124–126_a) and BF1-7 (BF 46–48), and the cryptotephra intervals (BF 154–156_a, BF 146–148, BF 116–118, BF 112–114, BF 104–106, BF 82–84), all exhibit a high-K calc-alkaline rhyolitic signature that based on TAS classification alone are chemically indistinguishable (Fig. 8). These tephra show considerable overlap with other calc-alkaline centres from central Turkish volcanic sources, e.g. Acıgöl, Erciyes Dağ, Göllü Dağ, and Hasan Dağ [commonly referred to as the Central Anatolian Volcanic Province (CAVP)]. However, the BF1 rhyolites may be tentatively distinguished from these, with plots of Al_2O_3 and TiO_2 wt.% proving particularly useful (Fig. 8). Single grain glass chemistry available from Armenian volcanic centres is limited, but analyses obtained as part of wider investigations by the authors suggest that the most consistent chemical overlap with the BF1 rhyolites are those

obtained from volcanic deposits mapped to the GVC (Fig. 8). Given the proximity of Gutansar to BF1 (Fig. 1A) and the abundance of glass shards identified within the studied sequence, it is most probable that the BF1 rhyolitic shards correlate to an eruptive episode(s) from this centre. However, the present limited knowledge with regard to the geochemistry of regional eruptive products precludes any firmer proposals regarding an exact source or timing of eruption(s) at present.

Alongside the primary population in BF1-5 (BF 124–126_a) are two further data clusters, denoted here as populations b and c. Population b has marginally higher TiO_2 values (c. 0.29 wt%), whereas population c has lower SiO_2 values (65–69 wt%) and higher Al_2O_3 (c. 17.7 wt%) compared to the primary population. It has not been possible to identify a chemical relative of these analyses, which probably reflects the incompleteness of the regional glass chemical dataset.

Glass shards comprising population a in BF1-3 (BF 142–144_a) and a single analysis from BF1-5 (BF 124–126_d) can be classified as trachyandesite (Fig. 8). Volcanic centres in the GVM are known to have produced trachyandesitic volcanic products during the Pleistocene (Arutyunyan *et al.*, 2007; Lebedev *et al.*, 2013), as have centres located in eastern Turkey [commonly referred to as the Eastern Anatolian Volcanic Province (EAVP) in recent scientific literature, e.g. Pearce *et al.*, 1990; Yilmaz *et al.*, 1998; Sumita and Schmincke, 2013a,b; Lebedev *et al.*, 2016a,b) and possibly the Syunik Highlands in southern Armenia (Kandel *et al.*, 2017). Given their relative proximity to BF1, these volcanic regions are among the most probable sources for BF1-3 (BF 142–144_a) and BF1-5 (BF 124–126_d). Single grain glass shard analyses are either not yet available from the intermediate products of the aforementioned regions, or are available in very low quantities, and while data are available from what is hypothesized to represent volcanic products from the Syunik Highlands (Kandel *et al.*, 2017), this link has not been proven chemically. At present, the greatest chemical similarity to BF1-3 (BF 142–144_a) and BF1-5 (BF 124–126_d) is exhibited by a tephra identified within Kalavan-2, a Middle Palaeolithic site c. 60 km NE of BF1 (Malinsky-Buller *et al.*, 2021). However, the age of the Kalavan-2 site means that it is too young to be a correlative of BF1, and it has not yet been possible to directly provenance the Kalavan tephra. Given the thickness of the BF1-3 and BF1-5 tephra horizons, their relatively coarse grain size, and the probable correlation of the rhyolitic tephra at BF1 to Gutansar, we argue it is most likely that BF1-3 (BF 142–144_a) and BF1-5 (BF 124–126_d) also originated from the proximal GVC.

Diatom analysis

Diatom results

A summary of the diatom assemblage is presented in Fig. 9 and the full dataset is included in Supporting Information S2. BF1-6 at 8.29–8.00 m is dominated by fluctuating levels of *Stephanodiscus medius* Håkansson and *Aulacoseira granulata* (Ehrenberg) Simonsen, with low but persistent occurrences of Narviculoid taxa. At 8.00 m, diatom concentrations fall, and thereafter remain low, with limited species diversity, until c. 7.85 m at which point concentrations of all diatom taxa rise notably. *A. granulata* initially dominates at 7.85 m, *S. medius* peaks at 7.70–7.65 m, there are first appearances of *Staurosirella pinnata* (Ehrenberg) Williams and Round, *Cocconeis placentula* spp. Ehrenberg and *Pseudostaurosira* species at 7.85 m, while Narviculoid taxa also increase in concentration. In BF1-7 (7.60–7.56 m) all diatom concentrations are reduced because of the dilution of the sediment by volcanic ash discussed above. However, concentrations return to higher levels above 7.55 m, with *S. medius* dominating the assemblage between 7.54 and

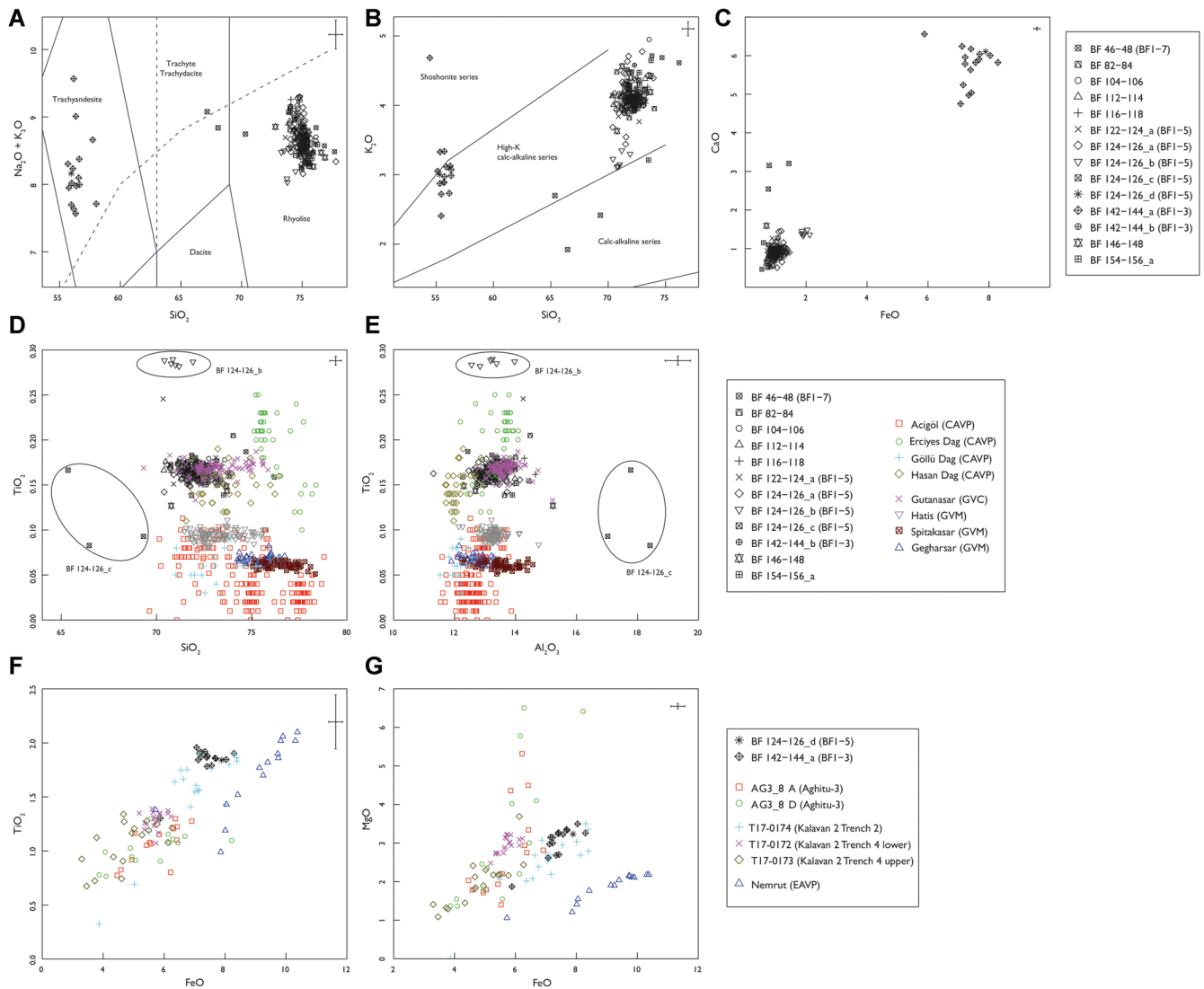


Figure 8. Selected chemical plots illustrating non-normalized major element glass chemistry of Bird Farm visible ashes and cryptotephra. The Bird Farm sequence is dominated by glass shards of an indistinguishable high-K calc-alkaline rhyolitic signature. These are probably of local origin and can be tentatively correlated to the Gutansar volcano located within the proximal GVC, despite some similarities to centres in the CAVP. (A) Total alkali silica classification based on normalized data (Le Bas *et al.*, 1986). Biplots B-G show selected major element glass chemistry from BF1 compared to selected sequence and volcanic centres in the region. (B) SiO_2 vs. K_2O (wt. %) based on non-normalized data (Peccerillo and Taylor, 1976). (C) FeO vs. CaO (wt. %). (D) SiO_2 vs. TiO_2 (wt. %). (E) Al_2O_3 vs. TiO_2 (wt. %). (F) FeO vs. TiO_2 (wt. %). (G) FeO vs. MgO (wt. %). Comparative data derived from Slimak *et al.* (2008), Tryon *et al.* (2009), Schmitt *et al.* (2011), Tomlinson *et al.* (2015), Kandel *et al.* (2017), Malinsky-Buller *et al.* (2021) and the authors unpublished data. Error bars represent 2 SD of replicate analyses of Lipari ($n=47$; plots A-E) and BCR2g ($n=53$; plots F and G) glass standards.

7.33 m (BF1-8), while *A. granulata* occurs at lower, but consistent levels. *Pseudostaurosira* species are also present in consistent but low quantities, while *S. pinnata* and *C. placentula* spp. initially occur in lower concentrations than at 7.85–7.65 m before increasing above 7.32 m.

Diatom interpretation

The diatom record indicates that the strata formed in a deep, temperate, alkaline lake, with high nutrient availability (Rioual *et al.*, 2007), the latter probably linked to a high concentration of incorporated silicic tephra shards. Variations in the dominance between the two key species, *S. medius* and *A. granulata*, are probably linked to variations in the length and timing of spring and autumn lake overturning, with *S. medius* thriving during episodes of intense and prolonged springtime mixing (Bradbury *et al.*, 2002; Rioual *et al.*, 2007). In contrast, the heavily silicified *A. granulata* requires higher temperatures, alongside deep mixing, to keep the heavily silicified taxa in the photic zone and is thus often found in lakes with strong autumn overturning. Both species require nutrient-rich waters

(Kilham *et al.*, 1986; O'Farrell *et al.*, 2001), and they often appear to track one another, with high concentrations indicating periods of intensified spring and autumn overturning, both of which allow nutrient resuspension (Winder and Hunter, 2008), and hence a reduced period of summer stratification. Evident through the lower part of BF1-6 is a relatively consistent diatom assemblage indicating lake stability, with limited changes in lake stratification regime and/or physico-chemical properties of the water column. A notable shift in the diatom assemblage is evident at 7.85 m, represented by a significant increase in the occurrence of benthic taxa above this depth. Two possible mechanisms could explain the change: (i) an extension of the euphotic zone, favouring benthic diatom production (Wolin and Duthie, 1999), or (ii) a change in lake productivity or biodiversity, resulting in an increase in benthic diatom productivity (Althouse *et al.*, 2014; Leira *et al.*, 2015). The continued presence of a relatively high proportion of benthic taxa through the upper part of BF1-6 and BF1-8 represents the continuation of relative lake stability, albeit associated with differing lake conditions.

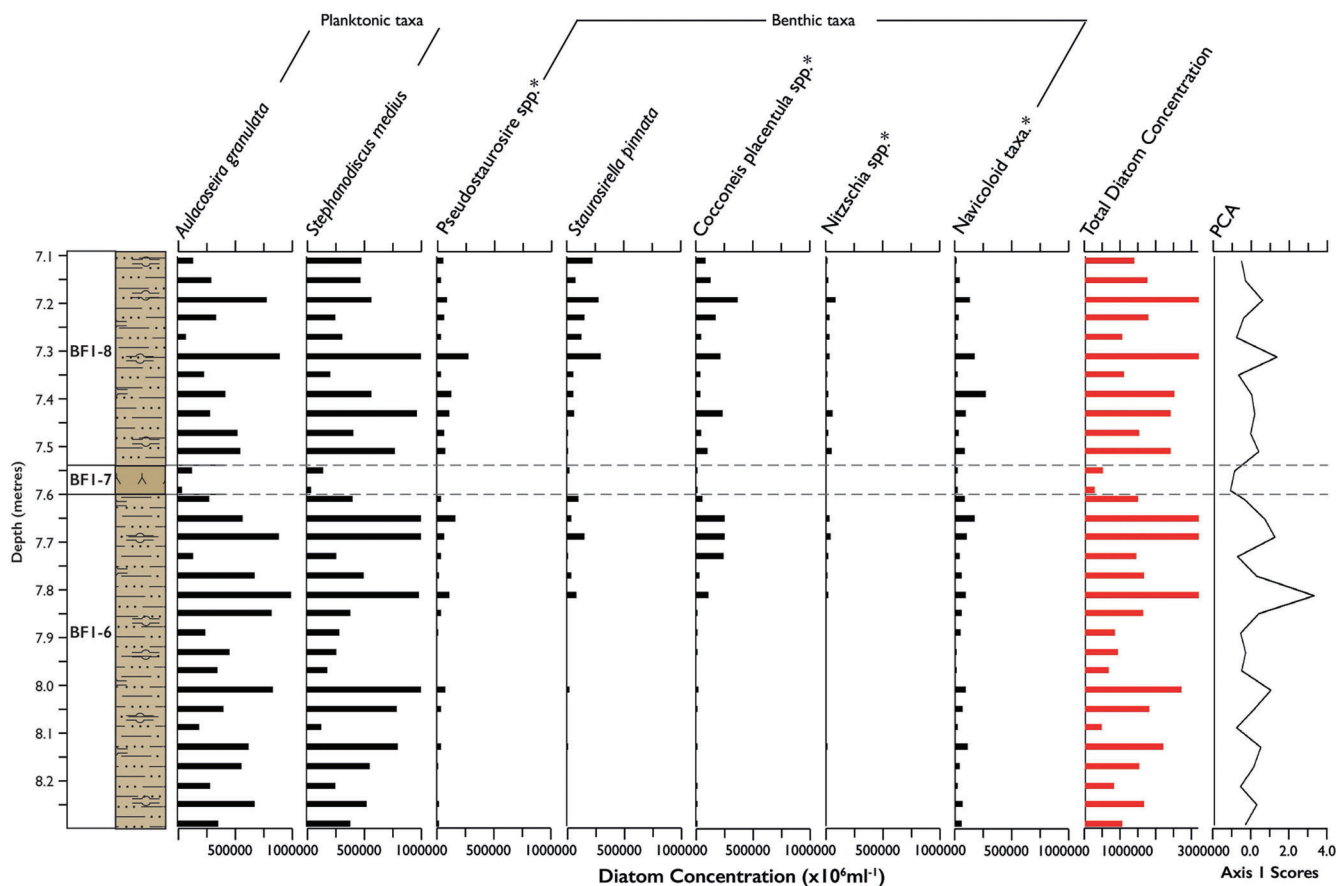


Figure 9. Summary diatom assemblage data for BF1-6 to BF1-8. Shown are the principal planktonic and benthic data, diatom concentration and axis 1 scores of the PCA.

Landscape and environmental change at Bird Farm 1 and in the Hrazdan valley

The sequence at BF1 provides evidence for changes in both lacustrine sedimentation and depositional environment in the Hrazdan gorge during the Middle Pleistocene. Broadly, the sequence represents two phases of deposition during which there were three primary tephra falls, the basal two separated from the upper by an interval of subaerial exposure. The second phase of lacustrine sedimentation is followed by a period of alluvial activity and pedogenesis before capping of the sequence by lava emplacement (Table 2). As outlined in 'Geological and site context', a broad chronology for landscape development at BF1 is provided by $^{40}\text{Ar}/^{39}\text{Ar}$ age estimates derived from the lava flow (BF1-11) that caps the deposits and lava flows HGW-VI and HGW-IV outcropping at NG1. It is important to note that attempts were made to $^{40}\text{Ar}/^{39}\text{Ar}$ date the visible tephra BF1-3 and BF1-7 as part of this study. Extraction of minerals (feldspar) followed the protocol outlined in Adler *et al.* (2014); however, it was not possible to obtain the required number of crystals of an appropriate size for accurate $^{40}\text{Ar}/^{39}\text{Ar}$ dating. However, the age of the BF1 sequence can be further refined by correlation of the deposits with those at NG1 (Fig. 10). $^{40}\text{Ar}/^{39}\text{Ar}$ dating of sanidines derived from the upper sediment stratum (Unit 1) at NG1 has yielded an age of 308 ka, while that layer in turn directly overlies a series of pedogenically modified alluvial deposits (NG1 Units 2–5). We argue that the latter are floodplain and levee facies of the same stream that deposited the BF1-9 channel sediments. Accepting this hypothesis would imply that the BF1 sequence accumulated in the interval 440–308-ka, with pedogenic development at BF1 occurring

contemporaneously with NG1 during Marine Isotope Stage (MIS) 9e. Given the correlation of the upper alluvial strata at BF1 to MIS 9e we hypothesize lake persistence at BF1 is associated with an earlier interval of warmer conditions, possibly during MIS 11.

The earliest phase of lacustrine sedimentation (BF1-1 to BF1-5) is associated with the development of a shallow lacustrine system after 440 ka. Lake formation probably occurred as a response to impeded drainage in the Hrazdan basin and due to damming of the palaeo-Hrazdan by lava flow emplacement (Sherriff *et al.*, 2019). Associated with this phase were at least three intervals of volcanic activity, represented by the two visible primary airfall deposits (BF1-3 and BF1-5) and the reworked felsic ash within BF1-2. The particle size distribution and close chemical similarity with proximal deposits from the GVM suggest that a local volcanic centre (e.g. Gutansar) is the probable source of the primary and reworked tephra. Together, the presence of a high volume of volcanic material and allochthonous siliclastic sediment in the lower strata of the BF1 sequence indicates a highly dynamic landscape in which large volumes of easily erodible material lay on the land surface surrounding the basin. Consequently, the lacustrine system was subject to a large amount of inwashing and rapid sediment deposition.

The second phase of landscape evolution at BF1 is represented by the weathered upper stratum of BF1-5, indicating a reduction in water level in the lacustrine system, subaerial weathering of the tephra, and with clay illuviation. Formation of this surface represents a depositional hiatus in the BF1 sequence. The cause of the change in water level is, however, not clear from the sedimentary evidence alone. It may in part be a consequence of infilling of the basin through

Table 2. Synthesis of landscape development at BF1 and in the wider Hrazdan valley based on sedimentological, geochemical and biological evidence from the BF1 sequence. Presented is the model of sedimentary input at BF1, the inferred depositional environment and hypothesized geomorphic changes in the Hrazdan valley. Where applicable, the proposed sources of volcanic material and inferred hydroclimate conditions are stated. Chronology is based on $^{40}\text{Ar}/^{39}\text{Ar}$ ages from BF1 and NG1 (Adler *et al.*, 2014; Sherriff *et al.*, 2019).

Unit	Sedimentary input	Tephra source	Bird Farm depositional environment	Hrazdan valley geomorphic event	Hydroclimate reconstruction	Inferred chronology
Phase 6 BF1-10	Mafic lava		Lava emplacement	Effusive volcanic activity in NW GVM. Lava flows in palaeo-Hrazdan valley.		195 ± 8 ka 198 ± 7 ka MIS 7
Unconformity- Phase 5 BF1-9b	Siliciclastic (<i>in situ</i> weathering)		Pedogenesis	Soil development on palaeo-Hrazdan floodplain	Temperate conditions	MIS 9e*
Phase 4 BF1-9a & BF1-9b	Siliciclastic – coarse grained (allochthonous)		Fluvial system (in channel).	Infill/drainage of lake system. Re-initiation of palaeo-Hrazdan fluvial system		MIS 9e*
Unconformity - Phase 3 BF1-8	Siliciclastic – fine grained diatom-rich (autochthonous)		Deep, stratified lacustrine system. High phytoplankton productivity and some allochthonous inputs from aeolian sources and periodic events.	Impeded drainage in Hrazdan basin downstream of BF1. Lake formation in BF1 locale.	Temperate conditions. Evidence for at least one phase of enhanced lake productivity.	MIS 11
BF1-7 BF1-6	Tephra fall (primary) Siliciclastic – fine grained diatom-rich (autochthonous)	GVM/CAVP/EAVP				
Unconformity - Phase 2 BF1-5	Siliciclastic (<i>in situ</i> weathering)		Incipient pedogenesis.	Cessation of lake system due to infilling or lake drainage.		MIS 11
Phase 1 BF1-5 BF1-4	Tephra fall (primary) Siliciclastic – fine grained (allochthonous)	Cutansar (proximal)	Shallow lacustrine system. High sediment yield from inwashing of volcanic material and primary tephra falls.	Impeded drainage in Hrazdan basin. Lake formation in BF1 locale. Explosive volcanic activity in NW GVM		
BF1-3 BF1-2 BF1-1	Tephra fall (primary) Tephra fall (reworked) Siliciclastic – fine grained (allochthonous) Emplacement of HGW-IV in western Hrazdan Gorge	Cutansar (proximal) GVM/CAVP/EAVP				441 ± 6 ka MIS 12

*An MIS 9e age for BF1-9 and BF1-10 is proposed based on correlation to NG1.

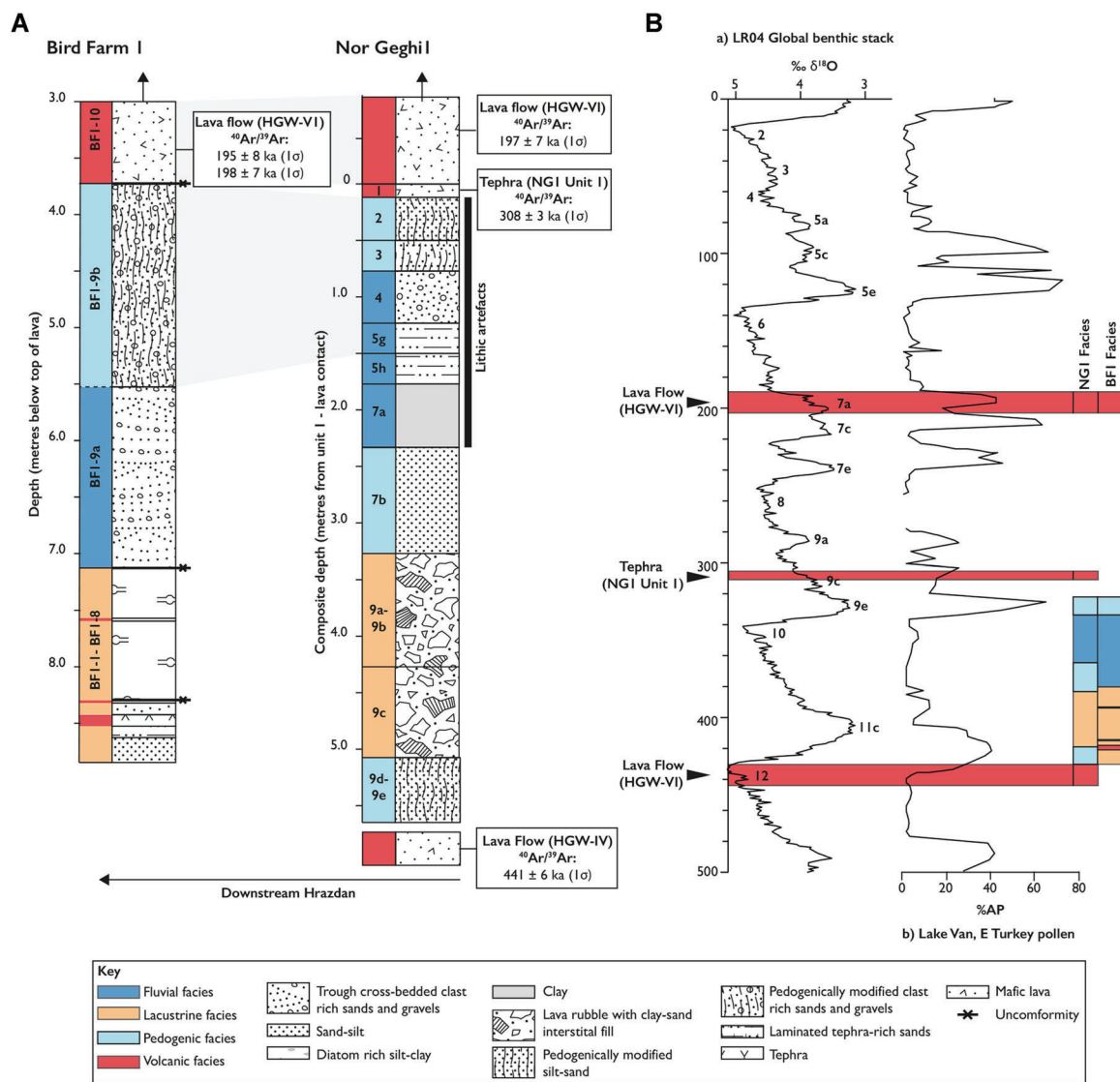


Figure 10. Schematic showing hypothesized correlations of (A) the BF1 and NG1 (Adler *et al.*, 2014) sequence, and (B) BF1 and NG1 with the global marine isotope stratigraphy (LR04; Lisecki and Raymo, 2004) and Lake Van arboreal pollen record (Litt *et al.*, 2014). Upper NG1 stratigraphy (Units 1–4) is based primarily on that reported by Adler *et al.* (2014). The lower stratigraphy (Units 5g–9e) is based on more recent excavations at NG1 (D. S. Adler and K. N. Wilkinson, unpublished data). Lava cobbles with silt–clay interstitial fill (Units 9a–e) in the NG1 sequence are interpreted to represent the lacustrine facies. For both BF1 and NG1 the principal fluvial, lacustrine, pedogenic and volcanic facies are highlighted in A and correlated to the regional stratigraphies in B. As described in the main text, we hypothesize that the upper fluvial and pedogenic facies in BF1 (BF1–9) are lateral equivalents to the upper fluvial and pedogenic facies at NG1 (Units 2–5) and are probably correlated to MIS 9e. The underlying lacustrine, volcanic and fluvial facies at both sites were therefore probably deposited during the interval 440–320 ka (MIS 11–10) on the basis of the ³⁹Ar/⁴⁰Ar dating of the lava flow (HGW-IV) that forms the base of the NG1 sequence.

the rapid deposition of volcanic material. Alternatively, it could represent a reduction in water level as a response to climatic (aridity) or, more probably, geomorphic processes related to damming of the lake elsewhere in the catchment (Sherriff *et al.*, 2019).

The third phase of landscape evolution recorded in the BF1 sequence is represented by a return to lacustrine sedimentation, albeit associated with a deeper, stratified water body. It is likely that this new lake system formed because of the damming of the palaeo-Hrazdan downstream of the BF1 locale. The formation of a deep lake system involves: (i) the presence of a basin of a significant depth to contain the waterbody (e.g. a valley) and (ii) a significant inflow of water. By implication it was likely that there was not a barrier to palaeo-Hrazdan flow upstream of the BF1 locale at this time. Sedimentological, geochemical and diatom evidence indicate the persistence of a deep, stratified lake with periodic seasonal overturning in a warm climate. This indicates lake persistence under relatively stable environmental conditions, with

allochthonous inputs principally from aeolian sources and periodic inwashing events. At least one primary pyroclastic airfall event is recorded during the interval (BF1–7), which given the chemical similarity of this ash unit to the tephra in the rest of the sequence may indicate a GVM eruptive source, although Turkish eruptive sources (e.g. the CAVP) cannot be excluded.

The combined diatom and geochemical evidence from the BF1 sequence indicates at least one interval of changing lake conditions during this third phase. This change was manifested by an increase in benthic diatom taxa occurring contemporaneously with enhanced organic content and Si production, a relative reduction in allochthonous inputs and a greater level of anoxia. Together, these lines of evidence suggest an extension of the euphotic zone, resulting in enhanced lake productivity and a shift in lake trophic status (Althouse *et al.*, 2014; Leira *et al.*, 2015). There are several possible explanations for this: (i) a reduction in lake level because of climatic change (enhanced warming and/or aridity) or geomorphic processes

resulting in the extension and development of aquatic vegetation (e.g. Ruhland *et al.*, 2015), (ii) a reduction in lake turbulence because of falling wind strength, favouring the development of benthic diatom communities (e.g. Wang *et al.*, 2012) or (iii) a reduction in the duration or change in timing of ice-cover, enhancing light availability and nutrient availability.

The fourth phase of landscape evolution in the BF1 locale represents the onset of alluvial deposition, characterized by the moderate-energy in-channel fluvial sedimentation. Given the unconformity between the alluvial sediments and underlying lacustrine strata, it is not clear when this activity occurred. Nevertheless, we can hypothesize that the depositional shift to a fluvial style was probably a consequence of breaching of the dam downstream of the BF1 locale, resulting in drainage of the lake system and the commencement of fluvial activity and floodplain development in the Hrazdan valley. The gravels forming the BF1 fluvial deposits have a diverse lithology, representing the wide range of Quaternary and pre-Quaternary geologies outcropping in the modern Upper Hrazdan valley (Sherriff *et al.*, 2019), indicating that the fluvial system (probably the palaeo-Hrazdan) had a comparable catchment to the modern Hrazdan. This interval of alluvial activity was followed by soil development on the palaeo-Hrazdan floodplain, which probably occurred alongside the development of climax vegetation communities in MIS 9e. The final phase of Pleistocene landscape evolution recorded at BF1 is lava emplacement, this latter representing the final period of effusive volcanic activity affecting the Hrazdan gorge at 200 ka (MIS 7). Previous mapping of this lava flow indicates that it originated from either the Gutansar, Hatis or Menaksar edifices located on the eastern side of the Hrazdan valley (Sherriff *et al.*, 2019).

Discussion

Palaeoenvironmental significance of the Bird Farm sequence

The combined sedimentological, geochemical and diatom evidence from BF1 provides a record of environmental conditions during the Middle Pleistocene. There is evidence for two phases of sediment accumulation under temperate conditions, albeit associated with differing depositional regimes, and at least four intervals of changing hydrological conditions in the Hrazdan Basin around the BF1 locale. Significantly, the BF1 record provides the first quantitative diatom evidence for changing environmental conditions in the Armenian Highlands (and the wider southern Caucasus) during the Middle Pleistocene.

Given the chronology of the site, we hypothesize that the temperate conditions recorded at BF1 represent separate interglacial periods, MIS 9e and MIS 11c. The former is represented by the development of mature Bk horizons, indicating floodplain soil formation and probably associated with the development of climax vegetation communities under fully interglacial conditions, while the latter is represented by the persistence of a deep lake system under warm conditions. Significantly, shifts observed during this interval of lake persistence may hint at changes in temperature or precipitation regime *within* MIS 11. While we are keen to avoid over-interpretation given ambiguities in elucidating the driver(s), and timing of this shift, the evidence highlights the potential of lacustrine systems for recording sub-Milankovitch environmental changes in the southern Caucasus.

The prevalence of warm and humid interglacial conditions in the Hrazdan valley during the Middle Pleistocene supports

the limited palaeoenvironmental evidence from the region. Malacological evidence from loess–palaeosol sequences in northern Armenia indicates the development of forest steppe during interglacials indicating increased humidity and warm conditions in comparison with semi-arid to arid conditions during glacial periods (Richter *et al.*, 2020). These sites lie at a much lower elevation (c. 400 m asl) than the Hrazdan valley. However, pollen evidence from Lake Van, which is at a comparable altitude to the Hrazdan valley (1647 m asl), albeit 180 km to the south-west and separated from BF1 by the Armenian Highlands, also indicates enhanced warmth and increased humidity during Middle Pleistocene interglacials, as evidenced by the development of mixed-oak steppe (Litt *et al.*, 2014).

The hydrological changes recorded in the BF1 sequence cannot be interpreted on the basis of climate alone, given the strong geomorphic and volcanic control on the Hrazdan valley throughout the Pleistocene (Sherriff *et al.*, 2019). Rather, these hydrological changes are hypothesized to be linked to changing sediment supply and impeded drainage of the palaeo-Hrazdan upstream and downstream of the BF1 locale, both of which are closely related to the volcanic history of the basin. Indeed, the evidence from BF1 supports the broad sediment succession recorded elsewhere in the Hrazdan valley of lava emplacement damming the Hrazdan valley and lake formation, a shift to fluvial deposition as a function of breaching of the lava dam or base-level change, floodplain development and subsequent lava emplacement. Evident in the BF1 sequence, however, is more complexity in the pattern of geomorphic change, with evidence for the occurrence of two distinct lake systems in the Hrazdan gorge during the interval 440–200 ka. While it is not possible from the geomorphic evidence to account for the causes of these changes, it does imply changes to the pattern of the drainage of the palaeo-Hrazdan on at least two occasions before the onset of fluvial deposition at the BF1 locale.

Tephrostratigraphical significance of the Bird Farm sequence

The BF1 sequence records the first Middle Pleistocene tephrostratigraphy to be published from the Armenian Highlands. Evident in the sequence are three stratigraphically distinct tephra layers each representing separate eruptive events/phases, while there are also high concentrations of cryptotephra throughout. Overlapping chemical signatures of the cryptotephra, supported by micromorphology and sedimentological evidence, suggests that the record represents the local reworking of volcanic deposits derived from the GVM. High background concentration of volcanic glass in the sequence therefore acts to mask any primary tephra deposition, meaning distinct eruptive episodes are unlikely to be identified in the cryptotephra record.

The visible tephra in the BF1 sequence therefore provides the best means for tephrostratigraphic correlation. Major element glass chemistry of these tephra indicates potential eruptive sources in Turkey and the GVM. However, given the thickness of the BF1-3, BF1-5 and BF1-7 tephra horizons, a local source is favoured. Radiometric (K–Ar) and FT dating of obsidian and other felsic deposits proximal to the edifice of Gutansar provides an estimated interval of activity between 550 and 200 ka (Oddone *et al.*, 2000; Badalian *et al.*, 2001; Karapetian *et al.*, 2001; Lebedev *et al.*, 2011, 2013), overlapping with the formation of the BF1 sequence (440–200 ka). However, we cannot currently exclude other volcanic centres in the western GVM (e.g. Hatis and Menaksar) given that they also have eruptive phases spanning this Middle Pleistocene

interval (Badalian *et al.*, 2001; Karapetian *et al.*, 2001; Lebedev *et al.*, 2013) while their glass chemistry is at present incompletely resolved.

Potential correlations of the visible tephra in the BF1 sequence, and indeed other Pleistocene sequences from the Armenian Highlands and broader Caucasus region (e.g. Malinsky-Buller *et al.*, 2021), with known source areas is more problematic for three reasons: (i) the chemical similarity of tephra derived from different local and regional volcanic sources on the basis of their major element chemistry; (ii) incomplete understanding of the timing and chemical signature of eruptions from local volcanic centres in Armenia, specifically those in the GVM and AVM, which have chronologies indicating eruptive episodes during the Pleistocene (Chernyshev *et al.*, 2002; Lebedev *et al.*, 2011; Meliksetian *et al.*, 2014); and (iii) the absence of single-shard glass data from distal volcanic centres that also have eruptive histories spanning the Middle Pleistocene [e.g. Elbrus (Greater Caucasus), Damavand (Iranian Plateau) Nemrut, Suphan Tendurek (eastern Turkey)]. Despite these uncertainties, the tephrostratigraphy at BF1 offers considerable potential for the correlation of sediment sequences within the Hrazdan Valley and beyond. Indeed, such isochrons will be of particular significance if they can be linked to tephra associated with archaeological sites (e.g. Kagshi 1: Sherriff *et al.*, 2019; lower strata in NG1: Adler *et al.*, 2014). Specifically, the tephrostratigraphic correlation of archives that contain palaeoenvironmental proxy evidence, such as BF1, will allow for the future development of a framework linking landscape, environmental and archaeological changes in the Armenian Highlands and the southern Caucasus as a whole.

Bird Farm and the Hrazdan valley archaeological record

The BF1 sequence cannot yet be firmly correlated with hominin activity at NG1 or indeed elsewhere, a situation that will persist until either tephra-derived isochrons can be established or absolute ages are obtained for the BF1 tephra (either directly by $^{40}\text{Ar}/^{39}\text{Ar}$ or indirectly by chronologies derived elsewhere). However, on the assumption that the fluvial channel strata at BF1 (BF1-9) are facies equivalents of the floodplain deposits at NG1 (Units 1–4), it can in turn be inferred that the lacustrine beds at BF1 are lateral equivalents of lake sediment outcropping beneath the alluvial layers at NG1 (Fig. 10) (D. S. Adler and K. N. Wilkinson, unpublished data). Furthermore, acceptance of such an inference would imply that the lake stretched at least 1.7 km north-eastwards from the BF1 locale. It is also of note that the earliest Palaeolithic artefacts at NG1 are associated with rubble derived from the 440 ka HGW-IV lava, while lake sediments have formed around the trachyandesite cobbles and boulders (D. S. Adler and K. N. Wilkinson). These data have significant implications for the interpretation of the initial hominin activity at NG1 that will be considered elsewhere, but suffice to say that lake margin settings were utilized by hominin groups throughout the Early and Middle Pleistocene (e.g. Blumenschine *et al.*, 2012; Roach *et al.*, 2016; Stewart *et al.*, 2020). They are recognized as ecotonal environments that allow both freshwater and adjacent terrestrial settings to be exploited, while at the same time being a location for the congregation of potential prey. Indeed, the high nutrient status of the BF1 lake suggests that it would have been a rich source of aquatic resources, particularly during its deep-water phase. At a broader level, the posited BF1-NG1 correlation would confirm previously published suggestions that Lower and early Middle Palaeolithic occupations in the Caucasus region are archaeologically most visible during interglacials (Adler *et al.*, 2014; Sherriff *et al.*, 2019), periods which, as discussed above, are argued to have been warm and humid. Even so, excepting NG1 and Koudaro III

in South Ossetia (Doronichev, 2011), Palaeolithic sites in the region have yet to be chronometrically dated to the MIS 11–9 interval, albeit that several are known from the MIS 7 interglacial (e.g. Azokh cave in Nagorno-Karabakh: Fernández Yalvo *et al.*, 2010; Asryan *et al.*, 2014; Djrchula, Georgia: Mercier *et al.*, 2010). The tephrostratigraphic approach outlined above may in the future enable correlation of the BF1 stratigraphy with the wider Middle Pleistocene archaeological record.

Conclusions

- The Bird Farm-1 sequence represents the first record for the Armenian Highlands that combines sedimentological, tephrostratigraphical and diatom data to reconstruct Middle Pleistocene environmental and landscape change in the region.
- We have demonstrated six phases of landscape development in the Hrazdan gorge between successive lava flow emplacements at 440 and 197 ka and comprising the development of at least two distinct lacustrine systems, separated by an interval of subaerial weathering. Deposition in a lacustrine setting was followed by an interval of fluvial activity and subsequent land surface stability. Within the sequence is evidence for at least two intervals of sediment accumulation under warm conditions, which, on the basis of the Hrazdan valley stratigraphy (Sherriff *et al.*, 2019), we hypothesize to be MIS 9e and MIS 11c.
- Diatom data from the sequence provide evidence for fluctuating lake conditions during one of these intervals and which might be linked to changing climate regimes within a single warm phase. While further proxy evidence is needed to fully understand these changes, the record demonstrates the strong potential for fragmentary lake sequences (such as BF1) in the Caucasus region to record Middle Pleistocene climatic changes. This result is of particular significance in a region where highly dynamic tectonism means that the likelihood of finding long, continuous lacustrine sequences spanning large parts of the Pleistocene is low.
- Major element chemical characterization of three visible tephra and six cryptotephra horizons in the sequence represents the first published stage in the development of a regional tephrostratigraphy for the Middle Pleistocene. The chemistry of the visible tephra horizons suggests derivation from Armenian and Turkish sources. Combined stratigraphical, chronological and glass shard geochemical evidence from two of these tephra allows for the tentative correlation to proximal deposits of the GVM volcano, Gutansar, c. 10 km NE of the site.
- Together, the diatom and tephra evidence demonstrate that linkages can be established between palaeoenvironmental archives at both a local (Hrazdan valley) and regional (Armenian Highlands and Caucasus) scale. Such connections will enable us to better understand the environmental backdrop of the expansion, behavioural change and evolution of Middle Pleistocene hominins in the region generally.

Supporting information

Additional supporting information can be found in the online version of this article. This article includes online-only Supplemental Data.

S1. Tephra chemistry raw datasets, summary table and standards data.

S2. Diatom concentrations and raw counts.

Acknowledgements. We thank Dr Khachatur Meliksetian (Director of the Institute of Geological Sciences, RA Academy of Sciences) and Dr Dmitri Arakelyan (Institute of Geological Sciences, RA Academy of Sciences), Dr Pavel Avetisyan (Director of the Institute of Archaeology and Ethnography, RA Academy of Sciences) and Karen Bayramyan (Head of the Protection of Monuments of History and Culture Agency for the Ministry of Culture, Republic of Armenia) for their insights on the archaeology and geology of central Armenia and for logistical help. We are also very grateful to Suren Kesejian for his invaluable assistance in the field and elsewhere, and the Partevian family for hosting us during fieldwork. Dr Monika Knul (University of Winchester), Jayson Gill (University of Connecticut), Alexander Brittingham (University of Connecticut), Yannick Raczyński-Henk and Dr Phil Glauberman are also thanked for their help in the field. Finally we thank two anonymous reviewers for their constructive comments on an earlier version of the paper. The analyses and a significant part of the fieldwork reported here was funded by the Leverhulme Trust (RPG-2016-102), while the University of Connecticut's Norian Armenian Programs Committee and the Gfoeller Renaissance Foundation, USA, also provided financial assistance.

Abbreviations. AVM, Aragats volcanic massive; BF1, Bird Farm 1; CAVP, Central Anatolian Volcanic Province; EAVP, Eastern Anatolian Volcanic Province; FT, Fission Track; GVC, Gutansar Volcanic Complex; GVM, Gegham volcanic massive; MIS, Marine Isotope Stage MS, magnetic susceptibility; NG1, Nor Geghi 1.

References

- Abich G. 1845. *Über die geologische Natur des Armenischen Hochlandes*. Druck Von Heinrich Laakmann: Dorpat.
- Acopian Center for the Environment. 2019. Vector database Armenia. American University of Armenia. www.acopiancenter.am/GISPortal/. (Accessed 16/2/2021).
- Adler DS, Bar-Oz G, Belfer-Cohen A *et al.* 2006. Ahead of the game: Middle and Upper Palaeolithic hunting practices in the Southern Caucasus. *Current Anthropology* **47**: 89–118. <https://doi.org/10.1086/432455>
- Adler DS, Bar-Yosef O, Belfer-Cohen A *et al.* 2008. Dating the demise: Neanderthal extinction and the establishment of Modern Humans in the Southern Caucasus. *Journal of Human Evolution* **55**: 817–833. <https://doi.org/10.1016/j.jhevol.2008.08.010> [PubMed: 18930307]
- Adler DS, Wilkinson KN, Blockley S *et al.* 2014. Early Levallois technology and the Lower to Middle Paleolithic transition in the Southern Caucasus. *Science* **345**: 1609–1613. <https://doi.org/10.1126/science.1256484> [PubMed: 25258079]
- Althouse B, Higgins S, Vander, Zanden MJ. 2014. Benthic and planktonic primary production along a nutrient gradient in Green Bay, Lake Michigan, USA. *Freshwater Science* **33**: 487–498. <https://doi.org/10.1086/676314>
- Arutyunyan EV, Lebedev VA, Chernyshev IV *et al.* 2007. Geochronology of Neogene–Quaternary volcanism of the Geghama Highland (Lesser Caucasus, Armenia). *Doklady Earth Sciences* **416**: 1042–1046. <https://doi.org/10.1134/S1028334X07070136>
- Asryan L, Ollé A, Moloney N *et al.* 2014. Lithic assemblages of Azokh Cave (Nagorno Karabagh, Lesser Caucasus): raw materials, technology and regional context. *Journal of Lithic Studies* **1**: 33–54. <https://doi.org/10.2218/jls.v1i1.775>
- Bailey RG. 1989. *Bailey Ecoregions Map of the Continents*. World Conservation Monitoring Center: Cambridge. <https://www.unep-wcmc.org/resources-and-data/baileys-ecoregions-of-the-world>
- Bakker L, Lowe DJ, Jongmans AG. 1996. A micromorphological study of pedogenic processes in an evolutionary soil sequence formed on Late Quaternary rhyolitic tephra deposits, North Island, New Zealand. *Quaternary International* **34–36**: 249–261. [https://doi.org/10.1016/1040-6182\(95\)00090-9](https://doi.org/10.1016/1040-6182(95)00090-9)
- Bar-Yosef O, Belfer-Cohen A, Adler DS. 2006. The implications of the Middle–Upper Paleolithic chronological boundary in the Caucasus to Eurasian Prehistory. *Anthropologie* **XLIV**: 81–92.
- Bar-Yosef O, Belfer-Cohen A, Mesheviliani T *et al.* 2011. Dzudzuana: an Upper Palaeolithic cave site in the Caucasus foothills (Georgia). *Antiquity* **85**: 331–349. <https://doi.org/10.1017/S0003598X0006779X>
- Battarbee R, Juggins S, Gasse F *et al.* 2001. An information system for palaeoenvironmental reconstruction. *EDDI* **81**: 1–94.
- Blockley SPE, Pyne-O'Donnell SDF, Lowe JJ *et al.* 2005. A new and less destructive laboratory procedure for the physical separation of distal glass tephra shards from sediments. *Quaternary Science Reviews* **24**: 1952–1960. <https://doi.org/10.1016/j.quascirev.2004.12.008>
- Blumenschine RJ, Masao FT, Stollhofen H *et al.* 2012. Landscape distribution of Oldowan stone artifact assemblages across the fault compartments of the eastern Olduvai Lake Basin during early lowermost Bed II times. *Journal of Human Evolution* **63**: 384–394. <https://doi.org/10.1016/j.jhevol.2011.05.003> [PubMed: 21945135]
- Bradbury P, Cumming B, Laird K. 2002. A 1500-year record of climatic and environmental change in Elk Lake, Minnesota III: Measures of past primary productivity. *Journal of Paleolimnology* **27**: 321–340. <https://doi.org/10.1023/A:1016035313101>
- Bullock P, Fedoroff N, Jongerius A *et al.* 1985. *Handbook for Soil Thin Section Description*. Waine Research.
- Cullen VL, Smith VC, Tushabramishvili N *et al.* 2021. A revised AMS and tephra chronology for the Late Middle to Early Upper Paleolithic occupation of Ortvale Klde, Republic of Georgia. *Journal of Human Evolution* **151**: 102908. <https://doi.org/10.1016/j.jhevol.2020.102908>
- Das SK, Routh J, Roychoudhury AN *et al.* 2009. Phosphorus dynamics in shallow eutrophic lakes: an example from Zeekoevlei, South Africa. *Hydrobiologia* **619**: 55–66. <https://doi.org/10.1007/s10750-008-9600-0>
- Dearing JA. 1999. Magnetic susceptibility In *Environmental Magnetism; a Practical Guide*. Quaternary Research Association Technical Guide No. 6, Walden J, Oldfield F, Smith J (eds.). Quaternary Research Association: London.
- Dearing JA, Dann RJL, Hay K *et al.* 1996. Frequency-dependent susceptibility measurements of environmental materials. *Geophysical Journal International* **124**: 228–240. <https://doi.org/10.1111/j.1365-246X.1996.tb06366.x>
- Djamali M, de Beaulieu JL, Shah-Hosseini M *et al.* 2008. A late Pleistocene long pollen record from Lake Urmia, NW Iran. *Quaternary Research* **69**: 413–420. <https://doi.org/10.1016/j.yqres.2008.03.004>
- Fernández-Jalvo Y, King T, Yepiskoposyan L *et al.* (eds). 2016. *Azokh Cave and the Transcaucasian Corridor*. Vertebrate Paleobiology and Paleoanthropology Series. Springer: Dordrecht.
- Ferring R, Oms O, Agustí J *et al.* 2011. Earliest human occupations at Dmanisi (Georgian Caucasus) dated to 1.85–1.78 Ma. *Proceedings of the National Academy of Sciences of the United States of America* **108**: 10432–10436. <https://doi.org/10.1073/pnas.1106638108> [PubMed: 21646521]
- Frahm E, Feinberg JM, Schmidt-Magee BA *et al.* 2016. Middle Palaeolithic toolstone procurement behaviors at Lusakert Cave 1, Hrazdan Valley, Armenia. *Journal of Human Evolution* **91**: 73–92. <https://doi.org/10.1016/j.jhevol.2015.10.008> [PubMed: 26852814]
- Frahm E, Jones CO, Corolla M *et al.* 2020. Comparing Lower and Middle Palaeolithic lithic procurement behaviors within the Hrazdan basin of central Armenia. *Journal of Archaeological Science: Reports* **32**: 102389.
- Frahm E, Sherriff J, Wilkinson KN *et al.* 2017. Ptghni: a new obsidian source in the Hrazdan River basin, Armenia. *Journal of Archaeological Science: Reports* **14**: 55–64. <https://doi.org/10.1016/j.jasrep.2017.05.039>
- Gabunia L, Antón SC, Lordkipanidze D *et al.* 2001. Dmanisi and dispersal. *Evolutionary Anthropology* **10**: 158–170. <https://doi.org/10.1002/evan.1030>
- Gasparyan B, Egeland CP, Adler DS *et al.* 2014. The Middle Paleolithic occupation of Armenia: summarizing old and new data. In *Stone Age of Armenia*, Gasparyan B, Arimura M (eds.). Center for Cultural Resource Studies, Kanazawa University; 65–106.
- Gehrels MJ, Newnham RM, Lowe DJ *et al.* 2008. Towards rapid assay of cryptotephra in peat cores: review and evaluation of various methods. *Quaternary International* **178**: 68–84. <https://doi.org/10.1016/j.quaint.2006.10.014>
- Gevorgyan H, Breikreuz C, Meliksetian K *et al.* 2020. Quaternary ring plain- and valley-confined pyroclastic deposits of Aragats strato-volcano (Lesser Caucasus): lithofacies, geochronology and eruption history. *Journal of Volcanology and Geothermal Research* **401**: 106928. <https://doi.org/10.1016/j.jvolgeores.2020.106928>
- Gile LH. 1961. A classification of Ca horizons in soils of a desert region, Dona Ana County, New Mexico. *Soil Science Society of*

- America Journal* **25**: 52–61. <https://doi.org/10.2136/sssaj1961.03615995002500010024x>
- Gill JL, Williams JW, Jackson ST *et al.* 2012. Climatic and megaherbivory controls on late-glacial vegetation dynamics: a new, high-resolution, multi-proxy record from Silver Lake, Ohio. *Quaternary Science Reviews* **34**: 66–80. <https://doi.org/10.1016/j.quascirev.2011.12.008>
- Glauber P, Gasparyan B, Sherriff J *et al.* 2020b. Barozh 12: formation processes of a late Middle Paleolithic open-air site in western Armenia. *Quaternary Science Reviews* **236**: 106276. <https://doi.org/10.1016/j.quascirev.2020.106276>
- Glauber P, Gasparyan B, Wilkinson KN *et al.* 2020a. Late Middle Paleolithic technological organisation and behaviour at the open-air site of Barozh 12 (Armenia). *Journal of Paleolithic Archaeology* **3**: 1095–1148. <https://doi.org/10.1007/s41982-020-00071-4>
- Golovanova LV, Doronichev VB, Cleghorn NE *et al.* 2010. Significance of ecological factors in the Middle to Upper Paleolithic Transition. *Current Anthropology* **51**: 655–691. <https://doi.org/10.1086/656185>
- Guiry MD, Guiry GM. 2018. *AlgaeBase*. www.algaebase.org. (Accessed 9/8/2020).
- Halama R, Meliksetian K, Savov IP *et al.* 2020. Pinched between the plates: Armenia's voluminous record of volcanic activity. *Geology Today* **36**: 101–108. <https://doi.org/10.1111/gto.12309>
- Hall M, Hayward C. 2014. Preparation of micro- and crypto-tephras for quantitative microbeam analysis. *Geological Society, London, Special Publications* **398**: 21–28. <https://doi.org/10.1144/SP398.5>
- Heiri O, Lotter AF, Lemcke G. 2001. Loss on ignition as a method for estimating organic and carbonate content in sediments: reproducibility and comparability of results. *Journal of Paleolimnology* **25**: 101–110. <https://doi.org/10.1023/A:1008119611481>
- Huang J, Kang S, Zhang Q *et al.* 2013. Atmospheric deposition of trace elements recorded in snow from the Mt. Nyainqêntanglha region, southern Tibetan Plateau. *Chemosphere* **92**: 871–881. <https://doi.org/10.1016/j.chemosphere.2013.02.038> [PubMed: 23535470]
- Joannin S, Cornée JJ, Münch P *et al.* 2010. Early Pleistocene climate cycles in continental deposits of the Lesser Caucasus of Armenia inferred from palynology, magnetostratigraphy, and $^{40}\text{Ar}/^{39}\text{Ar}$ dating. *Earth and Planetary Science Letters* **291**: 149–158. <https://doi.org/10.1016/j.epsl.2010.01.007>
- Kalińska E, Nartišs M. 2014. Pleistocene and Holocene aeolian sediments of different location and geological history: A new insight from rounding and frosting of quartz grains. *Quaternary International* **328–329**: 311–322. <https://doi.org/10.1016/j.quaint.2013.08.038>
- Kandel AW, Gasparyan B, Allué E *et al.* 2017. The earliest evidence for Upper Paleolithic occupation in the Armenian Highlands at Aghitu-3 Cave. *Journal of Human Evolution* **110**: 37–68. <https://doi.org/10.1016/j.jhevol.2017.05.010> [PubMed: 28778461]
- Karapetian SG, Jrbashian RT, Mnatsakanian AKh. 2001. Late collision rhyolitic volcanism in the north-eastern part of the Armenian Highland. *Journal of Volcanology and Geothermal Research* **112**: 189–220. [https://doi.org/10.1016/S0377-0273\(01\)00241-4](https://doi.org/10.1016/S0377-0273(01)00241-4)
- Karapetyan KI, Adamyan AA. 1973. *Noveyshiy vulkanizm nekotorykh Rayonov Armyanskoy SSR (Younger Volcanism of Some Regions of the Armenian SSR)*. Armenian Academy of Sciences Publishing House: Yerevan (in Russian).
- Kemp AES. 1996. Laminated sediments as paleoindicators. In *Palaeoclimatology and Palaeoceanography from Laminated Sediments*, Kemp AES (ed.), *Geological Society Special Publication* **116**: vii–xii.
- Kharazyan H. 2005. *Geological map of Republic of Armenia*, Kharazyan H (ed.). Ministry of Nature Protection of Republic of Armenia: Yerevan.
- Kilham P, Kilham SS, Hecky RE. 1986. Hypothesized resource relationships among African planktonic diatoms. *Limnology and Oceanography* **31**: 1169–1181. <https://doi.org/10.4319/lo.1986.31.6.1169>
- Krammer K. 2002. *Diatoms of Europe. Diatoms of the European Inland Waters and Comparable Habitats. Volume 3: Cymbella*. Germany.
- Krammer K, Lange-Bertalot H. 1986. *Bacillariophyceae. 1: Teil: Naviculaceae*, Süßwasserf (ed.). Gustav Fischer Verlag: Stuttgart.
- Krammer K, Lange-Bertalot H. 1988. *Bacillariophyceae. 2: Teil: Bacillariaceae, Epithemiaceae, Surirellaceae*, Süßwasserf (ed.). Gustav Fischer Verlag: Stuttgart.
- Krammer K, Lange-Bertalot H. 1991a. *Bacillariophyceae. 3: Teil: Centrales, Fragilariaceae, Eunotiaceae*, Süßwasserf (ed.). Gustav Fischer Verlag: Stuttgart.
- Krammer K, Lange-Bertalot H. 1991b. *Bacillariophyceae. 4: Teil: Achnantheaceae*, Süßwasserf (ed.). Gustav Fischer Verlag: Stuttgart.
- Kylander ME, Klaminder J, Wohlfarth B *et al.* 2013. Geochemical responses to paleoclimatic changes in southern Sweden since the late glacial: the Hässeldala Port lake sediment record. *Journal of Paleolimnology* **50**: 57–70. <https://doi.org/10.1007/s10933-013-9704-z>
- le Bas MJ, Maitre RWL, Streckeisen A *et al.* 1986. A chemical classification of volcanic rocks based on the total alkali-silica diagram. *Journal of Petrology* **27**: 745–750. <https://doi.org/10.1093/petrology/27.3.745>
- Lange-Bertalot H. 2001. *Diatoms of Europe: Diatoms of the Europe inland waters and comparable habitats. Volume 2: Navicula sensu stricto, 10 Genera separated from Navicula sensu lato*, Frustulia. ed. Germany.
- Lebedev VA, Chernyshev IV, Shatagin KN *et al.* 2013. The Quaternary volcanic rocks of the Geghama Highland, Lesser Caucasus, Armenia: geochronology, isotopic Sr–Nd characteristics, and origin. *Journal of Volcanology and Seismology*. **7**: 204–229. <https://doi.org/10.1134/S0742046313030044>
- Lebedev VA, Chernyshev IV, Yakushev AI. 2011. The initiation time and the duration of Quaternary magmatism in the Aragats neovolcanic area, Lesser Caucasus, Armenia. *Doklady Earth Sciences* **437**: 808–812.
- Lebedev VA, Chugaev AV, Ünal E *et al.* 2016b. Late Pleistocene Tendürek volcano (Eastern Anatolia, Turkey). II. Geochemistry and petrogenesis of the rocks. *Petrology* **24**: 234–270. <https://doi.org/10.1134/S0869591116030048>
- Lebedev VA, Sharkov EV, Ünal E *et al.* 2016a. Late Pleistocene Tendürek volcano (Eastern Anatolia, Turkey): I. Geochronology and petrographic characteristics of igneous rocks. *Petrology* **24**: 127–152. <https://doi.org/10.1134/S0869591116020041>
- Leira M, Filippi ML, Cantonati M. 2015. Diatom community response to extreme water-level fluctuations in two Alpine lakes: a core case study. *Journal of Paleolimnology* **53**: 289–307. <https://doi.org/10.1007/s10933-015-9825-7>
- Lindbo DL, Stolt MH, Vepraskas MJ. 2010. Redoximorphic features. In *Interpretation of Micromorphological Features of Soils and Regoliths*, Stoops G, Marcelino V, Mees F (eds.). Elsevier: Amsterdam.
- Litt T, Anselmetti FS. 2014. Lake Van deep drilling project PALEOVAN. *Quaternary Science Reviews* **104**: 1–7. <https://doi.org/10.1016/j.quascirev.2014.09.026>
- Litt T, Pickarski N, Heumann G *et al.* 2014. A 600,000 year long continental pollen record from Lake Van, eastern Anatolia (Turkey). *Quaternary Science Reviews* **104**: 30–41. <https://doi.org/10.1016/j.quascirev.2014.03.017>
- Lordkipanidze D, Ponce de León MSP, Margvelashvili A *et al.* 2013. A complete skull from Dmanisi, Georgia, and the evolutionary biology of early. *Homo. Science* **342**: 326–331. <https://doi.org/10.1126/science.1238484> [PubMed: 24136960]
- Lowe DR. 1982. Sediment gravity flows; II. Depositional models with special reference to the deposits of high-density turbidity currents. *Journal of Sedimentary Research* **52**: 279–297.
- Malinsky-Buller A, Glauber P, Ollivier V *et al.* 2021. Short-term occupations at high elevation during the Middle Paleolithic at Kalavan 2 (Republic of Armenia). *PLoS ONE* **16**: e0245700. <https://doi.org/10.1371/journal.pone.0245700> [PubMed: 33539405]
- Malinsky-Buller A, Glauber P, Wilkinson KN *et al.* 2021. Evidence for Middle Palaeolithic occupation and landscape change in central Armenia at the open-air site of Alapars-1. *Quaternary Research* **99**: 223–247. <https://doi.org/10.1017/qua.2020.61>
- Martín-Puertas C, Valero-Garcés BL, Mata MP *et al.* 2011. Geochemical processes in a Mediterranean lake: a high-resolution study of the last 4,000 years in Zonar Lake, southern Spain. *Journal of Paleolimnology* **46**: 405–421. <https://doi.org/10.1007/s10933-009-9373-0>
- Miall AD. 1996. *The Geology of Fluvial Deposits*. Springer: Berlin.
- Moncel M-H, Pleurdeau D, Pinhasi R *et al.* 2015. The Middle Palaeolithic record of Georgia: a synthesis of the technological,

- economic and paleoanthropological aspects. *Anthropologie* **LIII**: 93–125.
- Müller J, Oberhänsli H, Melles M *et al.* 2001. Late Pliocene sedimentation in Lake Baikal: implications for climatic and tectonic change in SE Siberia. *Palaeogeography, Palaeoclimatology, Palaeoecology* **174**: 305–326. [https://doi.org/10.1016/S0031-0182\(01\)00320-0](https://doi.org/10.1016/S0031-0182(01)00320-0)
- Murray J, Domínguez-Alonso P, Fernández-Jalvo Y *et al.* 2010. Pleistocene to Holocene stratigraphy of Azokh 1 cave, Lesser Caucasus. *Irish Journal of Earth Sciences* **28**: 75–91. <https://doi.org/10.3318/IJES.2010.28.75>
- O'Farrell I, Tell G, Podlejski A. 2001. Morphological variability of *Aulacoseira granulata* (Ehr.) Simonsen (Bacillariophyceae) in the Lower Parana River (Argentina). *Limnology* **2**: 65–71. <https://doi.org/10.1007/s102010170001>
- Ollivier V, Fontugne M, Lyonnet B *et al.* 2016. Base level changes, river avulsions and Holocene human settlement dynamics in the Caspian Sea area (middle Kura valley, South Caucasus). *Quaternary International* **395**: 79–94. <https://doi.org/10.1016/j.quaint.2015.03.017>
- Ollivier V, Nahapetyan S, Roiron P *et al.* 2010. Quaternary volcano-lacustrine patterns and palaeobotanical data in southern Armenia. *Quaternary International* **223–224**: 312–326. <https://doi.org/10.1016/j.quaint.2010.02.008>
- Pearce JA, Bender JF, De Long SE *et al.* 1990. Genesis of collision volcanism in eastern Anatolia, Turkey. *Journal of Volcanology and Geothermal Research* **44**: 189–229. [https://doi.org/10.1016/0377-0273\(90\)90018-B](https://doi.org/10.1016/0377-0273(90)90018-B)
- Peccerillo A, Taylor SR. 1976. Geochemistry of Eocene calc-alkaline volcanic rocks from the Kastamonu area, northern Turkey. *Contributions to Mineralogy and Petrology* **58**: 63–81. <https://doi.org/10.1007/BF00384745>
- Peinerud EK. 2000. Interpretation of Si concentrations in lake sediments: three case studies. *Environmental Geology* **40**: 64–72. <https://doi.org/10.1007/PL00013330>
- Peti L, Gadd PS, Hopkins JL *et al.* 2020. Itrax μ -XRF core scanning for rapid tephrostratigraphic analysis: a case study from the Auckland Volcanic Field maar lakes. *Journal of Quaternary Science* **35**: 54–65. <https://doi.org/10.1002/jqs.3133>
- Pickarski N, Kwiecien O, Djmalı M *et al.* 2015. Vegetation and environmental changes during the last interglacial in eastern Anatolia (Turkey): a new high-resolution pollen record from Lake Van. *Palaeogeography, Palaeoclimatology, Palaeoecology* **435**: 145–158. <https://doi.org/10.1016/j.palaeo.2015.06.015>
- Pickarski N, Litt T. 2017. A new high-resolution pollen sequence at Lake Van, Turkey: insights into penultimate interglacial–glacial climate change on vegetation history. *Climate of the Past* **13**: 689–710. <https://doi.org/10.5194/cp-13-689-2017>
- Pilcher JR, Hall VA. 1992. Towards a tephrochronology for the Holocene of the north of Ireland. *Holocene* **2**: 255–259. <https://doi.org/10.1177/095968369200200307>
- Pinhasi R, Gasparian B, Nahapetyan S *et al.* 2011b. Middle Palaeolithic human occupation of the high altitude region of Hovk-1, Armenia. *Quaternary Science Reviews* **30**: 3846–3857. <https://doi.org/10.1016/j.quascirev.2011.09.020>
- Pinhasi R, Gasparian B, Wilkinson K *et al.* 2008. Hovk 1 and the Middle and Upper Paleolithic of Armenia: a preliminary framework. *Journal of Human Evolution* **55**: 803–816. <https://doi.org/10.1016/j.jhevol.2008.04.005> [PubMed: 18930308]
- Pinhasi R, Higham TF, Golovanova LV *et al.* 2011a. Revised age of late Neanderthal occupation and the end of the Middle Paleolithic in the northern Caucasus. *Proceedings of the National Academy of Sciences of the United States of America* **108**: 8611–8616. <https://doi.org/10.1073/pnas.1018938108> [PubMed: 21555570]
- Pinhasi R, Nioradze M, Tushabramishvili N *et al.* 2012. New chronology for the Middle Palaeolithic of the southern Caucasus suggests early demise of Neanderthals in this region. *Journal of Human Evolution* **63**: 770–780. <https://doi.org/10.1016/j.jhevol.2012.08.004> [PubMed: 23084367]
- Pleurdeau D, Moncel M-H, Pinhasi R *et al.* 2016. Bondi Cave and the Middle-Upper Palaeolithic transition in western Georgia (south Caucasus). *Quaternary Science Reviews* **146**: 77–98. <https://doi.org/10.1016/j.quascirev.2016.06.003>
- Pyle DM. 1989. The thickness, volume and grain size of tephra fall deposits. *Bulletin of Volcanology* **51**: 1–15. <https://doi.org/10.1007/BF01086757>
- Reineck H-E, Singh IB. 1975. *Depositional Sedimentary Environments*. Springer: Berlin.
- Richter C, Wolf D, Walther F *et al.* 2020. New insights into Southern Caucasian glacial–interglacial climate conditions inferred from Quaternary gastropod fauna. *Journal of Quaternary Science* **35**: 634–649. <https://doi.org/10.1002/jqs.3204>
- Rioual P, Andrieu-Ponel V, de Beaulieu J-LL *et al.* 2007. Diatom responses to limnological and climatic changes at Ribains Maar (French Massif Central) during the Eemian and Early Würm. *Quaternary Science Reviews* **26**: 1557–1609. <https://doi.org/10.1016/j.quascirev.2007.03.009>
- Roach NT, Hatala KG, Ostrofsky KR *et al.* 2016. Pleistocene footprints show intensive use of lake margin habitats by *Homo erectus* groups. *Scientific Reports* **6**: 26374. <https://doi.org/10.1038/srep26374> [PubMed: 27199261]
- Roy PD, Jonathan MP, Pérez-Cruz LL *et al.* 2012. A millennial-scale Late Pleistocene–Holocene palaeoclimatic record from the western Chihuahua Desert, Mexico. *Boreas* **41**: 707–718. <https://doi.org/10.1111/j.1502-3885.2012.00266.x>
- Roy PD, Nagar YC, Juyal N *et al.* 2009. Geochemical signatures of Late Holocene paleo-hydrological changes from Phulera and Pokharan saline playas near the eastern and western margins of the Thar Desert, India. *Journal of Asian Earth Sciences* **34**: 275–286. <https://doi.org/10.1016/j.jseaes.2008.05.006>
- Roy PD, Rivero-Navarette A, Lopez-Balbiaux N *et al.* 2013. A record of Holocene summer–season palaeohydrological changes from the southern margin of Chihuahua Desert (Mexico) and possible forcings. *Holocene* **23**: 1105–1114. <https://doi.org/10.1177/0959683613483619>
- Roy PD, Smykatz-Kloss W, Sinha R. 2006. Late Holocene geochemical history inferred from Sambhar and Didwana playa sediments, Thar Desert, India: comparison and synthesis. *Quaternary International* **144**: 84–98. <https://doi.org/10.1016/j.quaint.2005.05.018>
- Schaller T, Christoph Moor HC, Wehrli B. 1997. Sedimentary profiles of Fe, Mn, V, Cr, As and Mo as indicators of benthic redox conditions in Baldeggersee. *Aquatic Sciences* **59**: 345–361. <https://doi.org/10.1007/BF02522363>
- Schmitt AK, Danišik M, Evans NJ *et al.* 2011. Acigöl rhyolite field, Central Anatolia, Central (part 1): high-resolution dating of eruption episodes and zircon growth rates. *Contributions to Mineralogy and Petrology* **162**: 1215–1231.
- Sedov S, Stoops G, Shoba S. 2010. Regoliths and soils on volcanic ash. In *Interpretation of Micromorphological Features of Soils and Regoliths*, Stoops G, Marcelino V, Mees F (eds.). Elsevier: Amsterdam; 275–304.
- Sherriff JE, Wilkinson KN, Adler DS *et al.* 2019. Pleistocene volcanism and the geomorphological record of the Hrazdan valley, central Armenia: linking landscape dynamics and the Palaeolithic record. *Quaternary Science Reviews* **226**: 105994. <https://doi.org/10.1016/j.quascirev.2019.105994>
- Slimak L, Kuhn SL, Roche H *et al.* 2008. Kaletpe Deresi 3 (Turkey): archaeological evidence for early human settlement in Central Anatolia. *Journal of Human Evolution* **54**: 99–111. <https://doi.org/10.1016/j.jhevol.2007.07.004> [PubMed: 17825358]
- Sosson M, Rolland Y, Müller C *et al.* 2010. Subductions, obduction and collision in the Lesser Caucasus (Armenia, Azerbaijan, Georgia), new insights. *Geological Society, London, Special Publications* **340**: 329–352.
- Spaulding SA, Bishop IW, Edlund MB *et al.* 2020. Diatoms of north America. <https://diatoms.org/>. (accessed 16/8/2020).
- Stewart M, Clark-Wilson R, Breeze PS *et al.* 2020. Human footprints provide snapshot of last interglacial ecology in the Arabian interior. *Science Advances* **6**: eaba8940. <https://doi.org/10.1126/sciadv.aba8940> [PubMed: 32948582]
- Stoops G, Marcelino V, Mees F (eds.). 2018. *Interpretation of Micromorphological Features of Soils and Regoliths*. Elsevier: Amsterdam.
- Stow DAV, Bowen AJ. 1980. A physical model for the transport and sorting of fine-grained sediment by turbidity currents. *Sedimentology* **27**: 31–46. <https://doi.org/10.1111/j.1365-3091.1980.tb01156.x>
- Sumita M, Schmincke HU. 2013b. Impact of volcanism on the evolution of Lake Van I: evolution of explosive volcanism of Nemrut

- Volcano (eastern Anatolia) during the past > 400,000 years. *Bulletin of Volcanology* **75**: 714. <https://doi.org/10.1007/s00445-013-0714-5>
- Sumita M, Schmincke HU. 2013b. Impact of volcanism on the evolution of Lake Van II: temporal evolution of explosive volcanism of Nemrut Volcano (eastern Anatolia) during the past ca. 0.4 Ma. *Journal of Volcanology and Geothermal Research* **253**: 15–34. <https://doi.org/10.1016/j.jvolgeores.2012.12.009>
- Telford RJ, Barker P, Metcalfe S *et al.* 2004. Lacustrine responses to tephra deposition: examples from Mexico. *Quaternary Science Reviews* **23**: 2337–2353. <https://doi.org/10.1016/j.quascirev.2004.03.014>
- Tomlinson EL, Smith VC, Albert PG *et al.* 2015. The major and trace element glass compositions of the productive Mediterranean volcanic sources: tools for correlating distal tephra layers in and around Europe. *Quaternary Science Reviews* **118**: 48–66. <https://doi.org/10.1016/j.quascirev.2014.10.028>
- Trigui Y, Wolf D, Sahakyan L *et al.* 2019. First calibration and application of leaf wax n-alkane biomarkers in loess-paleosol sequences and modern plants and soils in Armenia. *Geosciences* **9**: 263. <https://doi.org/10.3390/geosciences9060263>
- Tryon CA, Logan MAV, Mouralis D *et al.* 2009. Building a tephrostratigraphic framework for the Paleolithic of central Anatolia, Turkey. *Journal of Archaeological Science* **36**: 637–652. <https://doi.org/10.1016/j.jas.2008.10.006>
- Tushabramishvili N, Pleurdeau D, Moncel MH *et al.* 2012. Human remains from a new Upper Pleistocene sequence in Bondi Cave (Western Georgia). *Journal of Human Evolution* **62**: 179–185. <https://doi.org/10.1016/j.jhevol.2011.11.001> [PubMed: 22130184]
- Van den Bogaard C, Schmincke HU. 2002. Linking the North Atlantic to central Europe: a high-resolution Holocene tephrochronological record from northern Germany. *Journal of Quaternary Science* **17**: 3–20. <https://doi.org/10.1002/jqs.636>
- von Suchodoletz H, Gärtner A, Zielhofer C *et al.* 2018. Eemian and post-Eemian fluvial dynamics in the Lesser Caucasus. *Quaternary Science Reviews* **191**: 189–203. <https://doi.org/10.1016/j.quascirev.2018.05.012>
- Winder M, Hunter DA. 2008. Temporal organization of phytoplankton communities linked to physical forcing. *Oecologia* **156**: 179–192. <https://doi.org/10.1007/s00442-008-0964-7> [PubMed: 18274782]
- Wolf D, Baumgart P, Meszner S *et al.* 2016. Loess in Armenia – stratigraphic findings and palaeoenvironmental indications. *Proceedings of the Geologists' Association* **127**: 29–39. <https://doi.org/10.1016/j.pgeola.2016.02.002>
- Wolin JA, Duthie HC. 1999. Diatoms as indicators of water level changes in freshwater lakes. In *The Diatoms: Application for the Environmental and Earth Sciences*, Stoermer EF, Smol JP (eds.). University Press: Cambridge; 183–202.
- Yılmaz Y, Güner Y, Şaroğlu F. 1998. Geology of the Quaternary volcanic centres of the east Anatolia. *Journal of Volcanology and Geothermal Research* **85**: 173–210. [https://doi.org/10.1016/S0377-0273\(98\)00055-9](https://doi.org/10.1016/S0377-0273(98)00055-9)
- Zehetner F, Miller WP, West LT. 2003. Pedogenesis of volcanic ash soils in Andean Ecuador. *Soil Science Society of America Journal* **67**: 1797–1809. <https://doi.org/10.2136/sssaj2003.1797>